


## ORIGINAL ARTICLE

# TH1902, a new docetaxel-peptide conjugate for the treatment of sortilin-positive triple-negative breast cancer

Michel Demeule<sup>1</sup> | Cyndia Charfi<sup>1</sup> | Jean-Christophe Currie<sup>1</sup> | Alain Larocque<sup>1</sup> |  
Alain Zgheib<sup>2</sup> | Sophie Kozelko<sup>2</sup> | Richard Béliveau<sup>2</sup> | Christian Marsolais<sup>1</sup> |  
Borhane Annabi<sup>2</sup> 

<sup>1</sup>Theratechnologies Inc., Montréal, QC, Canada

<sup>2</sup>Laboratoire d'Oncologie Moléculaire, Université du Québec à Montréal, Montréal, QC, Canada

## Correspondence

Borhane Annabi, Département de chimie, Université du Québec à Montréal, C.P. 8888, Succ. Centre-ville, Montréal, QC H3C 3P8, Canada.  
Email: annabi.borhane@uqam.ca

## Funding information

This study was supported through funding by the Programme de Soutien à la Valorisation et au Transfert from the Quebec government, and by Theratechnologies Inc. and the Canadian Cancer Society funding opportunity on Breast Cancer Research through the SynergiQc program from the Consortium Québécois sur la Découverte du Médicament.

## Abstract

Triple-negative breast cancer (TNBC) is a heterogeneous subgroup of cancers which lacks the expression and/or amplification of targetable biomarkers (ie, estrogen receptor, progesterone receptor, and human epidermal growth factor receptor 2), and is often associated with the worse disease-specific outcomes than other breast cancer subtypes. Here, we report that high expression of the sortilin (SORT1) receptor correlates with the decreased survival in TNBC patients, and more importantly in those bearing lymph node metastases. By exploiting SORT1 function in ligand internalization, a new anticancer treatment strategy was designed to target SORT1-positive TNBC-derived cells both *in vitro* and in two *in vivo* tumor xenografts models. A peptide (TH19P01), which requires SORT1 for internalization and to which many anticancer drugs could be conjugated, was developed. *In vitro*, while the TH19P01 peptide itself did not exert any antiproliferative or apoptotic effects, the docetaxel-TH19P01 conjugate (TH1902) exerted potent antiproliferative and antimigratory activities when tested on TNBC-derived MDA-MB-231 cells. TH1902 triggered faster and more potent apoptotic cell death than did unconjugated docetaxel. The apoptotic and antimigratory effects of TH1902 were both reversed by two SORT1 ligands, neurotensin and progranulin, and on siRNA-mediated silencing of SORT1. TH1902 also altered microtubule polymerization and triggered the downregulation of the anti-apoptotic Bcl-xL biomarker. *In vivo*, both i.p. and i.v. administrations of TH1902 led to greater tumor regression in two MDA-MB-231 and HCC-70 murine xenograft models than did docetaxel, without inducing neutropenia. Altogether, the data demonstrates the high *in vivo* efficacy and safety of TH1902 against TNBC through a SORT1 receptor-mediated mechanism. This

**Abbreviations:** Bcl-xL, B-cell lymphoma-extra-large; D5W, 5% dextrose in water; DAPI, 4',6-diamidino-2-phenylindole; DIEA, diisopropylethylamine; DMSO, dimethylsulfoxide; EDTA, ethylenediaminetetraacetic acid; ER, estrogen receptor; FITC, fluorescein isothiocyanate; GAPDH, glyceraldehyde 3-phosphate dehydrogenase; HBSS, Hank's balanced salt solution; HER2, human epidermal growth factor receptor 2; IDC, infiltrating ductal carcinoma; IHS, immunohistochemical score; ILNC, involved lymph node carcinomas; KD, dissociation constant; MTD, maximal tolerated dose; NT, neurotensin; OS, overall survival; PARP, poly(ADP-ribose) polymerase; PBS, phosphate-buffered saline; PD-1, programmed cell death protein 1; PD-L1, programmed death ligand 1; PFS, progress-free survival; PI, propidium iodide; PR, progesterone receptor; SDS, sodium dodecyl sulfate; SORT1, sortilin; TBST, Tris-buffered saline containing Tween; TBTU, 2-(1H-Benzotriazole-1-yl)-1,1,3,3-tetramethylammonium tetrafluoroborate; TH1902, docetaxel-TH19P01-peptide; TMA, tissue microarray; TNBC, triple-negative breast cancer; UPLC/MS, ultra performance liquid chromatography/mass spectrometry; VPS10P, Vacuolar Protein Sorting 10 protein.

Michel Demeule and Cyndia Charfi contributed equally to this study.

This is an open access article under the terms of the Creative Commons Attribution-NonCommercial-NoDerivs License, which permits use and distribution in any medium, provided the original work is properly cited, the use is non-commercial and no modifications or adaptations are made.

© 2021 The Authors. *Cancer Science* published by John Wiley & Sons Australia, Ltd on behalf of Japanese Cancer Association.

property allows for selective treatment of SORT1-positive TNBC and makes TH1902 a promising avenue for personalized therapy with the potential of improving the therapeutic window of cytotoxic anticancer drugs such as docetaxel.

#### KEYWORDS

docetaxel, peptide-drug conjugate, receptor-mediated chemotherapy, sortilin, triple-negative breast cancer

## 1 | INTRODUCTION

Breast cancers are composed of several subtypes that share similar clinicopathological features, but that also exhibit several different biological characteristics. The major breast cancer subtypes reported from genomic studies include Luminal A and Luminal B cancer (both expressing hormone receptor-related genes), HER2-positive cancer associated with amplification of the human epidermal growth factor receptor 2 (HER2/ErbB2/neu) gene, and TNBC, which lacks expression of ERs, PRs or HER2.<sup>1,2</sup> Among breast cancers, 15%-20% express HER2, a receptor tyrosine kinase that is involved in the regulation of cellular growth.<sup>3</sup> In view of such tumor heterogeneity, it is unsurprising to observe variable clinical responses to current therapy treatments.

TNBC constitutes about 10%-20% of all types of breast cancers and is more common among young (<50 years old) black and Hispanic women, and those of low socioeconomic status.<sup>4,5</sup> Some other breast cancer risk factors include breastfeeding patterns and parity.<sup>6-9</sup> Histologically, TNBC represents 80%-90% of infiltrating ductal carcinomas but it is less common among the other subtypes, including medullary, metaplastic, secretory, adenoid cystic, and apocrine/histiocytic carcinomas.<sup>10</sup> Initially, TNBC was classified into six subtypes which, according to advances in sequencing technology, have been refined to the four following main subtypes based on recurrent genetic alterations, transcriptional patterns, and molecular features: basal-like 1 (BL1), basal-like 2 (BL2), mesenchymal (M), and luminal androgen receptor (LAR).<sup>11</sup> This classification currently represents the rationale for the emergence of new preclinical platforms, and prompts for the development of more precise targeted anticancer therapies.<sup>12</sup> Poor clinical prognosis is associated with TNBC characterized by its aggressiveness and high recurrence risks, especially during the first 5 years postdiagnosis.<sup>13-16</sup> It is further defined by its high likelihood to develop distant metastases, particularly in the lungs and the central nervous system.<sup>17</sup> Standard treatments for TNBC include cytotoxic chemotherapy based on the use of taxanes (paclitaxel, docetaxel, and cabazitaxel), anthracyclines (doxorubicin and epirubicin), and platinum derivatives (cisplatin and carboplatin).<sup>18-21</sup> These treatments can be combined with surgery and/or radiotherapy. However, despite high initial sensitivity to chemotherapy, not all treated patients demonstrate a favorable outcome, and only short progression-free survival (PFS) and overall survival (OS) have been reported.<sup>19,20,22</sup> Immunotherapy has gained unprecedented momentum with checkpoint inhibitors that show significant efficacy and a favorable toxicity profile for the treatment of solid tumors. However, TNBC is thought

to have a high frequency of genomic alteration and neoantigen formation. Pembrolizumab, which is a monoclonal anti-PD-1 antibody was tested in a phase 1b trial of 32 patients with PD-L1-positive TNBC and showed a modest response rate of 18.5%.<sup>23</sup> Investigational strategies, including the combination of different checkpoint inhibitors and the development of antibody-drug conjugates, are ongoing.<sup>24</sup> For patients whose tumors are PD-L1 positive, Tecentriq (atezolizumab) in combination with Abraxane (nab-paclitaxel) is available under accelerated approval. Two PARP inhibitors (olaparib and talazoparib) have also been approved for TNBC patients with germinal *BRCA1/2* mutation.<sup>25</sup> More recently, in 2020, Trodelvy, an antibody-drug conjugate that links the monoclonal antibody sacituzumab that targets the Trop-2 protein found in more than 90% of TNBC to the topoisomerase I inhibitor SN-38 chemotherapy, has also been approved for the treatment of adult patients with metastatic TNBC.<sup>26</sup> Nonetheless, TNBC, which is molecularly, clinically, and histologically heterogeneous, displays extremely severe outcomes compared to all other subtypes of breast cancers because of the lack of relevant drug targets and remains an area of high unmet medical need.

SORT1, also known as neurotensin receptor-3, is a membrane-bound receptor that belongs to the VPS10P family of receptors.<sup>27</sup> It is composed of an N-terminal extracellular VPS10 domain containing binding sites for different ligands, a transmembrane domain, and a short cytoplasmic domain containing two lysosomal sorting motifs.<sup>28</sup> SORT1 plays different roles associated with intracellular trafficking and sorting for various ligands, including neurotensin, progranulin, and apolipoprotein E.<sup>29-31</sup> Incidentally, SORT1 dysfunction is associated with many pathological diseases, including Alzheimer's disease, cardiovascular disease and atherosclerosis, and type 2 diabetes mellitus.<sup>32,33</sup> On the other hand, SORT1's upregulation has also been observed in many types of human cancers, such as breast, ovarian, pancreas, and melanoma, and in pituitary adenomas.<sup>27,34-38</sup> In particular, SORT1 has been reported to be expressed in 59% of TNBC.<sup>34</sup> Given the lack of specific targets for patients with TNBC, different strategies were explored to specifically target and exploit SORT1 receptor functions in TNBC. Thus, a vectorization therapy platform based on the use of a new peptide (TH19P01)-drug conjugate of docetaxel (TH1902) was developed. This strategy was used to first conjugate TH19P01 to doxorubicin (TH1904) and demonstrated high tolerability and efficacy in a human ovarian ES-2 tumor xenograft mouse model.<sup>39</sup> Here, our data strongly suggest that conjugation of docetaxel with TH19P01 leads to very efficient inhibition of TNBC tumor growth. The data also indicate that TH1902 treatment

should have a significant beneficial effect in patients suffering from SORT1-positive TNBC, and that TH1902 could well be rapidly envisioned as a new personalized therapy for this type of cancer.

## 2 | MATERIALS AND METHODS

### 2.1 | Animals

Animals were obtained from Charles River Laboratories, Inc. and allowed to acclimate for 5 days before experiments. Female CD-1 nude mice (CrI:NU-Foxn1<sup>nu</sup>, 20-25 g, 4-6 weeks old) were used for xenograft tumor models, female athymic nude mice (CrI:NU(NCr)-Foxn1<sup>nu</sup>, 20-25 g, 4-6 weeks old) were used in hematotoxicology and female CrI:CD-1 mice (25-30 g, 6-8 weeks old) were used for pharmacokinetic evaluation. All mice were maintained in a pathogen-free environment and handled in accordance with the Guidelines of the Canadian Council on Animal Care. Animal protocols were approved by the Institutional Animal Care and Use Committee of Université du Québec à Montréal.

### 2.2 | Reagents and antibodies

Human TNBC-derived MDA-MB-231, HCC-70 cells, and murine 4T1 mammary carcinoma cells were purchased from the American Type Culture Collection. MDA-MB-231/Luc cells were from Cell Biolabs, murine ID8 ovarian cancer cells were from Millipore (SCC145), and murine MC38 colon adenocarcinoma were from Kerfast. Cells were cultured according to the providers' instructions. For experiments, cells from frozen aliquots were resuscitated and subcultured for 5-10 passages. TH19P01 peptide and neurotensin were synthesized and purified in house with peptide purity >95%. Amino acids and resin for the peptide synthesis were from Matrix Innovation Inc. Progranulin was from Sigma-Aldrich. The Coomassie Plus Protein assay reagent and micro BCA protein assay kit were from Thermo Fischer Scientific. Antisortilin antibodies were from Abcam (Western blot, 1 µg/mL) and EMD Millipore (immunohistochemistry), anti-Bcl-xL (1:1000) was from Cell Signalling, and anti-GAPDH was from Advanced Immunochemical. AnnexinV and Propidium Iodide were from BD Pharmingen, anti- $\alpha$ -tubulin (1:2000) was from Sigma-Aldrich. Anti-mouse-Alexa<sup>488</sup> (1:1000), DAPI (2 µg/mL), and Prolong Gold antifade were from Thermo Fisher Scientific. Anti-mouse and anti-rabbit horseradish peroxidase-linked secondary antibodies were from Jackson ImmunoResearch Laboratories. The enhanced chemiluminescence reagent was from Denville Scientific Inc.

### 2.3 | Synthesis of docetaxel-TH19P01 peptide conjugate (TH1902)

DIEA (0.21 mL, 1.2 mmol) was added dropwise to a suspension of docetaxel (0.81 g, 1.0 mmol) and succinic anhydride (105 mg,

1.05 mmol) in DMSO (5 mL) under stirring. The mixture was stirred at room temperature and monitored by UPLC/MS. The reaction was completed after 2 hours. The solvent was removed, and the resulting residue was dissolved in dichloromethane and loaded on a Biotage silica column for purification. DoceSuOH was obtained as a white powder after lyophilization, and UPLC/MS analysis showed purity >95%. DIEA (0.234 mmol) was added dropwise to a solution of DoceSuOH (213 mg, 0.234 mmol) and TBTU (75 mg, 0.234 mmol) in DMSO (3-4 mL) in order to preactivate the DoceSuOH. The completion of preactivation was monitored by UPLC/MS, then a solution of TH19P01 peptide (Ac-GVRAKAGVRN(Nle)FKSESY, 120 mg, 0.062 mmol) in DMSO (0.2 mL) was added. The mixture was stirred at room temperature. The reaction was monitored by UPLC/MS until completion. The reaction mixture was purified using a 30RPC resin column and an AKTA purifier system (10%-80% ACN) to give TH19P01-(SuDoce)<sub>2</sub> or TH1902 as a white powder after lyophilization. Purity of the conjugate was evaluated by UPLC/MS and was >95% with a *m/z* mass of 3704 (1852.91, charge +2). The Bruker micro time of flight (microTOF) used to perform TH1902 analysis is paired with a Waters Acquity UPLC equipped with a diode array detectors and binary pump, and offers sophisticated focus technology to provide a combination of mass accuracy, resolution, and sensitivity with a mass range *m/z* 50-3000 Da.

### 2.4 | Tissue microarrays

SORT1 expression was evaluated using high-density TMAs (IMH-364; Novus Biologicals) of human breast cancer and normal adjacent tissues at the Institute for Research in Immunology and Cancer (Montreal, QC). These TMAs included normal adjacent tissues (*n* = 9 samples) and IDCs (*n* = 35 samples), and ILNCs (*n* = 10 samples). Furthermore, the TMAs included molecular subtype information allowing the assessment of SORT1 expression in TNBC (*n* = 19 samples). Immunostaining was performed on 4 µm sections of formalin-fixed paraffin-embedded tumor material. Briefly, slides were deparaffined using proprietary dewax reagents in xylene and then rehydrated with decreasing concentrations of ethanol followed by an endogenous peroxidase block. SORT1 antigen retrieval was performed by heat-induced epitope retrieval techniques with ER1 solution (Leica) for 30 minutes at 100°C. Mouse anti-SORT1 (clone F11) (EMD Millipore) primary antibody was incubated at 20 µg/mL for 30 minutes at room temperature. Target antigen was detected using the Bond Polymer Refine Detection (Leica) with diaminobenzidine chromogen for visualization according to the manufacturer's instructions. Sections were then counterstained with Leica proprietary hematoxylin and mounted for analysis. SORT1 labeling was scored by the IHS method on a scale ranging from 0 to 3 as follows: 0, negative staining; 1, weak staining; 2, moderate staining; 3, strong staining. The proportion of cells showing positive staining was recorded as follows: 1, none; 2, 10%-50%; 3, 50%-70%; 4, 70%-100%. The raw data were converted to the IHS by multiplying the quantity and staining intensity scores. Therefore, the IHS score ranged from 0 to 12.

## 2.5 | Western blot analysis

MDA-MB-231 cells were homogenized in lysis buffer (150 mM NaCl, 10 mM Tris-HCl, pH 7.4, 1 mM EDTA, 1 mM ethyleneglycol-O,O'-bis(2-aminoethyl)-N,N,N',N'-tetraacetic acid, 0.5% [vol/vol] Nonidet P-40 and 1% [vol/vol] Triton X-100) supplemented with a complete protease inhibitor cocktail from Calbiochem. Cells were incubated for 30 minutes at 4°C with vortex agitation every 5 minutes, sonicated and centrifuged at 15 000 g for 10 minutes at 4°C. Equal amounts of protein (20 µg) were separated by SDS-polyacrylamide gel electrophoresis. Proteins were then electrotransferred to a polyvinylidene fluoride membrane and blocked for 1 hour at room temperature using 5% nonfat dry milk in Tris-buffered saline (150 mM NaCl, 20 mM Tris-HCl, pH 7.5) containing 0.1% Tween-20 (TBST). Membranes were washed in TBST and incubated overnight with primary antibodies diluted in TBST containing 3% bovine serum albumin and 0.05% NaN<sub>3</sub>. Membranes were washed in TBST and incubated for 1 hour at room temperature with horseradish peroxidase-conjugated anti-mouse or anti-rabbit IgG (1/5000 dilution) in TBST containing 5% nonfat dry milk. Membranes were washed again in TBST and signals were detected using chemiluminescence (Amersham Biosciences).

## 2.6 | SORT1 gene silencing

MDA-MB-231 cells were transiently transfected for 24 hours with 200 nM of scrambled sequences (siCTL; AllStar Negative Control siRNA, 1027281) or specific human siRNA against SORT1 (siSORT1; Hs\_SORT\_4 FlexiTube siRNA: SI00073640; Qiagen) using Lipofectamine 2000 (ThermoFisher Scientific). The extent of protein knockdown was assessed by Western blotting as described above.

## 2.7 | Fluorescent Alexa<sup>488</sup>-labeled TH19P01 peptide binding and uptake assays

MDA-MB-231 cells were grown in 12-well plates in complete media for 24 hours. Cell surface binding of Alexa<sup>488</sup>-labeled TH19P01 peptide was performed on cells detached with PBS-citrate and resuspended in HBSS. Cells were incubated for 5 minutes at 4°C with increasing concentrations of Alexa<sup>488</sup>-labeled TH19P01 peptide (KD determination). For uptake experiments, siCTL- or siSORT1-transfected cells were washed with PBS and incubated in HBSS for 2 hours at 37°C in the presence or absence of 200 nM Alexa<sup>488</sup>-labeled TH19P01 peptide. Alexa<sup>488</sup>-labeled TH19P01 peptide uptake was also competed with or without an excess of unlabeled TH19P01 peptide (50 µM), neurotensin (10 µM) or progranulin (1.5 nM), or in cells pre-incubated for 15 minutes with increasing concentrations of the latter (Ki determination) and uptake performed for 30 minutes. Fluorescence was evaluated in the FL1 channel using a C6 Accuri flow cytometer (BD Biosciences). Cell surface binding was also confirmed and assessed by spectrofluorometry (ex 488/em 538, cut-off

530 nm) on adherent cells after 30 minutes of incubation at 4°C followed by a 20 minutes lysis in 1% SDS, and using a SpectraMax Gemini EM Microplate reader (Molecular Devices).

## 2.8 | Cell proliferation assay

To assess the effects of docetaxel and TH1902 on MDA-MB-231 and HCC-70 cell proliferation, cells (MDA-MB-231: 3000 cells/well, HCC-70: 7000 cells/well) were first seeded in 96-well plates (Perkin Elmer), then treated with various concentrations of drugs in complete cell culture medium. After 72 hours of incubation, cell proliferation was measured using the 3-(4,5-dimethylthiazol-2-yl)-2,5-diphenyltetrazolium bromide (MTT) assay in accordance with the protocol described by Mosmann with the following modifications.<sup>40</sup> The cells were incubated with MTT (0.5 mg/ml) at 37°C under a humidified atmosphere containing 5% CO<sub>2</sub> for 4 hours. After incubation, 100 µL of DMSO (solubilizing reagent) was added to each well and mixed thoroughly to dissolve the dark blue crystals. The presence of viable cells was visualized by the development of a purple color due to formation of formazan crystals. The plates were read on a SpectraMax Plus reader (Molecular Devices) using a test wavelength of 570 nm and reference wavelength of 630 nm. Analyses were made in quadruplicate for each condition.

## 2.9 | Cell cycle analysis

MDA-MB-231 cells were synchronised for 24 hours in serum-deprived media and then treated with vehicle, 4 µM docetaxel or 2 µM TH1902 (equimolar amount of docetaxel) for 2 hours, washed once, and further incubated with complete media for 22 hours. Cells were then detached with trypsin, centrifuged, and washed twice with PBS. One million cells were then resuspended in 0.3 mL of PBS, added to ice-cold 70% ethanol and incubated overnight at 4°C. Cells were pelleted, resuspended in PI (40 µg/mL)-RNase (100 µg/mL) solution for 30 minutes at 37°C, and analyzed for their DNA content in the FL2 channel using a BD Accuri C6 flow cytometer.

## 2.10 | Cell apoptosis assay

AnnexinV/PI staining was performed using an Apoptosis Detection Kit according to the manufacturer's instructions. Briefly, MDA-MB-231 cells were seeded for 24 hours in 12-well plates. In one experiment, cells were untreated or treated in serum-deprived media for 5 hours with various concentrations of docetaxel or TH1902. In another experiment, cells were incubated at 37°C in a serum-free media in the presence or absence of 5 µM TH1902 which was competed (or not) with an excess of unlabeled TH19P01 peptide (50 µM), neurotensin (10 µM) or progranulin (1 nM). After treatment, cells were harvested, resuspended at a density of 10<sup>6</sup> cells/mL in a staining solution of 100 µL of 1X binding buffer containing 5 µL of

AnnexinV-FITC and 5  $\mu$ L of PI. Cells were incubated for 15 minutes at room temperature in the dark before analysis by flow cytometry. The numbers of apoptotic cells were measured using the BD Accuri C6 software.

### 2.11 | Immunofluorescent staining

For  $\alpha$ -tubulin staining, cells were plated for 24 hours on glass coverslips and grown to 80% confluency. Cells were then treated for 24 hours with vehicle, 2  $\mu$ M docetaxel or 1  $\mu$ M TH1902 at 37°C, washed in PBS, fixed for 15 minutes in 4% paraformaldehyde, permeabilized with 1% Triton X-100 in PBS for 5 minutes, and finally washed in PBS. Cells were blocked in PBS containing 10% normal host serum and 0.05% Triton, and incubated for 1 hour with an anti- $\alpha$ -tubulin primary antibody. Cells were washed with PBS and incubated for 1 hour with Alexa-Fluor<sup>488</sup>-conjugated secondary antibody (1/1000; Invitrogen), washed with PBS, stained with DAPI (2  $\mu$ g/mL; Invitrogen) for 4 minutes, washed again in PBS and mounted onto slides using Prolong Gold antifade reagent. Cells were finally digitalized by confocal microscopy (Nikon A1) and analyzed using the NIH ImageJ Version 1.4.21 software.

### 2.12 | Real-time cell migration assay

Cell migration experiments were carried out using a real-time cell analyser dual-plate instrument, the xCELLigence system (Roche Diagnostics). This system was used according to the instructions of the manufacturer. Cells (25 000 cells/well) were seeded in serum-free medium onto a CIM-Plates 16 (Roche Diagnostics). These plates are similar to conventional Transwells (8- $\mu$ m pore size) with gold electrode arrays on the bottom side of the membrane, which provide a real-time measurement of cell migration. Prior to cell seeding, the underside of the wells from the upper chamber was coated with 25  $\mu$ L of 0.15% gelatin in PBS and incubated for 1 hour at 37°C. The lower chamber was filled with serum-free medium. The upper chamber of each well was filled with 100  $\mu$ L of MDA-MB-231 cells ( $2.5 \times 10^5$  cells/mL) previously transfected for 24 hours with siScrambled or siSORT1 and pretreated for 2 hours with or without 1  $\mu$ M TH1902 or 2  $\mu$ M free docetaxel (equimolar docetaxel concentration). After 30 minutes of adhesion, cell migration was monitored every hour for 12 hours. The impedance value was measured by the real-time cell analyser dual-plate instrument and was expressed as an arbitrary unit termed the "Cell Index" which reflects the number of actively migrating cells. Each experiment was performed in duplicate wells.

### 2.13 | *In vivo* therapeutic efficacy assessment of docetaxel and TH1902 in xenograft models

Tumor xenografts were established by subcutaneous inoculation of  $5 \times 10^6$  MDA-MB-231-Luc cells resuspended in 100  $\mu$ L of HBSS and

injected in the right flank of CD-1 nude mice under light isoflurane anaesthesia. When palpable tumors reached a volume of  $\sim 100$  mm<sup>3</sup>, mice were treated weekly with vehicle, docetaxel (15 mg/kg, MTD; i.p. five cycles, i.v. three cycles of treatments), or TH1902 (i.p. 50 mg/kg for five cycles; i.v. 8.75, 17.5 mg/kg for three cycles, and 35 mg/kg up to five cycles of treatments). Note that 35 mg/kg TH1902 and 15 mg/kg docetaxel contain equimolar amounts of docetaxel. For the i.p. study, tumor growth was evaluated as average bioluminescence levels in the different groups after mouse anaesthesia with isoflurane and 15 minutes following intraperitoneal D-luciferin injection (180 mg/kg) using the Xtreme Near Infrared Imaging system (Bruker Optics). Semiquantitative analysis was performed using MI Software version 5.0.5.29 (Bruker BioSpin). Identical illumination settings (exposure time, f/stop, filters, field of view, and binning) were used throughout image acquisition. All images were displayed in the same scale of fluorescence intensity. Fluorescence intensities were quantified using region of interest settings of equivalent sized areas. For the i.v. study, tumor growth was evaluated by two-dimensional measurements taken with an electronic caliper and tumor volume was calculated according to the following formula: tumor volume (mm<sup>3</sup>) =  $\pi/6 \times \text{length} \times \text{width}^2$ . Data are expressed as mean  $\pm$  SEM and were analysed using the GraphPad Prism Software.

### 2.14 | Hematotoxicity assay

Athymic nude mice were treated with docetaxel or TH1902 at a docetaxel-equivalent i.v. dose (15 mg/kg). Blood samples were collected in K3 EDTA micro tubes (Sarstedt) 4 days before the start of treatment, 4 days after the first and third treatments at docetaxel MTD, and 4 days after the first, third, and sixth treatments of TH1902. Blood neutrophil counts were performed on the day they were collected at the Diagnostic Laboratory of the Comparative Medicine Animal Resources Centre at McGill University.

### 2.15 | Pharmacokinetic analysis

Plasma samples for pharmacokinetic characterization were collected at 5, 15, and 30 minutes as well as at 1, 2, 4, and 6 hours following i.v. bolus injection of TH1902 into normal CD-1 mice with lithium heparin microvette tubes (Sarstedt). TH1902 and docetaxel concentrations were determined by UPLC/MS. Briefly, both TH1902 and docetaxel were extracted from 50  $\mu$ L of plasma using 4 volumes of cold acetonitrile (87%):acetic acid (0.125%):water (12.875%) in micro centrifuge tubes. After 5 minutes on ice, the suspensions were centrifuged at 10 000 g for 5 minutes and supernatants (2-10  $\mu$ L) were injected into a Waters Acquity UPLC spectrometer coupled to a microTOF spectrometer from Bruker using electron spray ionization (ESI-TOF). TH1902 and released docetaxel from the peptide were quantified by peak area ratio at a wavelength of 220 nm. Standard curves for TH1902 and docetaxel were performed in mouse plasma. A linear regression was carried out to determine the concentration



of TH1902 and docetaxel. The limit of quantitation for TH1902 and for free docetaxel was around 8  $\mu\text{M}$ .

## 2.16 | Statistical analysis

One-way ANOVA with Dunnet's post-test was used in all experiments involving comparison between multiple groups. Student's unpaired *t* test was used in experiments involving the comparison of control and siSORT1 groups. *P* values <.05 were considered significant. All analyses were performed using the GraphPad Prism software Version 5.0.

## 3 | RESULTS

### 3.1 | High SORT1 expression in breast cancers is associated with poor patient prognosis

SORT1 expression was first analyzed by immunohistochemistry in invasive IDCs, ILNCs, and TNBC samples, and compared to normal adjacent breast tissues. Representative SORT1 immunolabeling of samples from three different patients (Figure 1A) shows very low levels of SORT1 in normal adjacent tissues, whereas high levels of SORT1 labeling were observed in IDC, ILNC, and TNBC samples (Figure 1B).

Furthermore, *in silico* analysis of SORT1 gene expression on the survival of TNBC patients was performed using Kaplan-Meier plotter software (<http://kmplot.com/analysis/>) for patients expressing low or high SORT1 levels. Kaplan-Meier curves confirmed that high SORT1 gene expression is associated with a poor prognosis for TNBC patients in advanced 3 and 4 stages (Figure 2A). In addition, Kaplan-Meier analysis of TNBC patients with LNM shows a drastic effect of high SORT1 gene expression on patient survival (Figure 2B). This further supports SORT1 as a potential target in TNBC.

### 3.2 | SORT1 function is required for TH19P01 binding and uptake

SORT1-mediated cell surface binding and internalization of TH19P01 was first investigated in TNBC-derived MDA-MB-231 cells. Using

siRNA-mediated approaches, silencing of SORT1 was confirmed at the protein level by Western blotting (Figure 3A) and this was quantified by densitometry (Figure 3B). The binding and uptake of Alexa<sup>488</sup>-labeled TH19P01, at 4 and 37°C respectively, were also found to be significantly reduced by 59% and 72% on SORT1 silencing (Figure 3C). This demonstrates that functional SORT1 processes are required for both cell surface recognition and internalization of TH19P01. Binding of Alexa<sup>488</sup>-labeled TH19P01 was measured as a function of fluorescent peptide concentration and found saturable in MDA-MB-231 cells. The cell surface binding constant (KD) of TH19P01 was calculated at  $0.32 \pm 0.08 \mu\text{M}$  (Figure 3D). Next, inhibition of Alexa<sup>488</sup>-labeled TH19P01 uptake was performed with increasing concentrations of unlabeled TH19P01, TH1902, or NT (Figure 3E). Inhibition constants (Ki) were  $0.84 \pm 0.35 \mu\text{M}$ ,  $0.55 \pm 0.06 \mu\text{M}$ , and  $1.36 \pm 0.31 \mu\text{M}$  for TH19P01, TH1902, and NT respectively. These constants suggest that TH19P01 and TH1902 have affinities comparable to NT.

### 3.3 | Assessment of SORT1 expression requirement for TH19P01 peptide uptake in different cancer cell models

SORT1 expression and function in TH19P01 uptake were next assessed. Uptake of Alexa<sup>488</sup>-labeled TH19P01 was evaluated in human TNBC cells (MDA-MB-231), human colon cancer cells (MC38), murine ovarian cancer cells (ID8), and murine TNBC cells (4T1). Expression of SORT1 was high in MDA-MB-231 and ID8 cancer cells, whereas very low levels were found in MC38 and 4T1 cancer cells (Figure 4A,B, inserts). For further proof of concept of functional SORT1 involvement in TH19P01, excess concentrations of Sortilin's natural ligands were required in our *in vitro* assay to compete for SORT1-mediated Alexa<sup>488</sup>-labeled TH19P01 uptake. Such uptake was found inhibited in the presence of an excess of unlabeled TH19P01 and by the two SORT1 ligands, neurotensin and progranulin<sup>41,42</sup> only in those SORT1 expressing MDA-MB-231 (Figure 4A) and ID8 cells (Figure 4B). Basal TH19P01 uptake was low in cells that expressed low levels of SORT1, and excess SORT1 ligands were accordingly found inefficient to inhibit uptake (Figure 4A,B). Combined, these data confirm the involvement of SORT1 expression and function in the internalization process of TH19P01 within SORT1-positive cancer cell models.

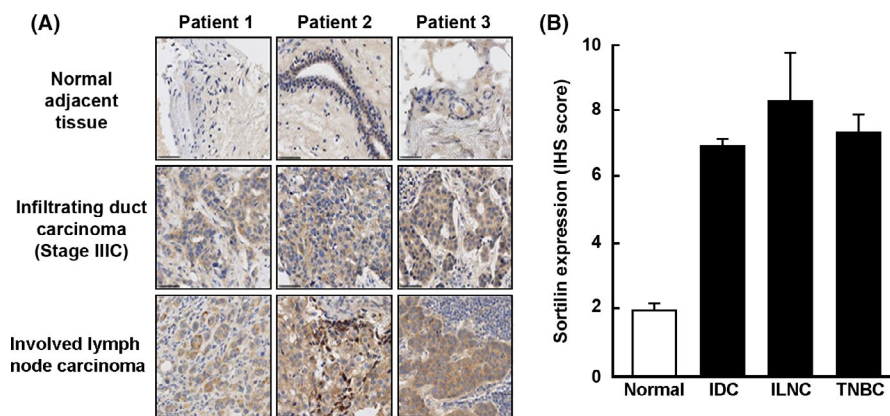


**FIGURE 1** SORT1 expression in breast cancers. A, Immunohistochemistry stainings were performed to assess SORT1 expression in normal adjacent tissue and in stage IIIC infiltrating duct carcinoma (IDC) and involved lymph node carcinoma (ILNC). B, SORT1 staining intensity was evaluated using the immunohistostaining (IHS) method on nine normal adjacent tissues, 35 IDC, 10 ILNC, and 19 TNBC tumors. Data are represented as mean  $\pm$  SEM

**FIGURE 2** In silico analysis of SORT1 gene expression on the survival of triple-negative breast cancer (TNBC) patients. (A) TNBC patient survival curves were obtained using the Kaplan-Meier plotter software (<http://kmpplot.com/analysis/>) for patients expressing low (black curve) or high (red curve) levels of *SORT1* ( $n = 161$  cases) or (B) in TNBC patients with lymph node metastases ( $n = 72$  cases)

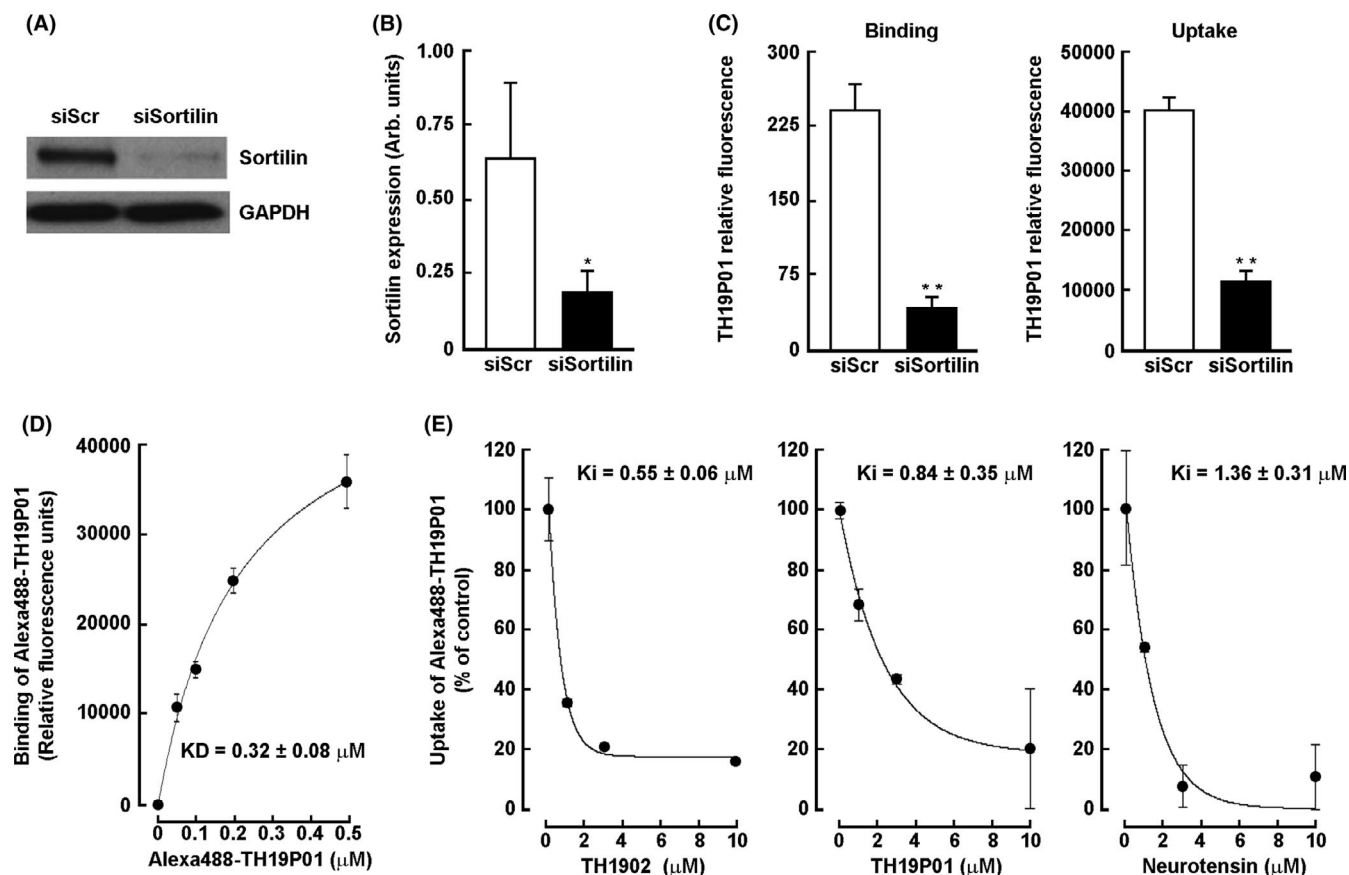
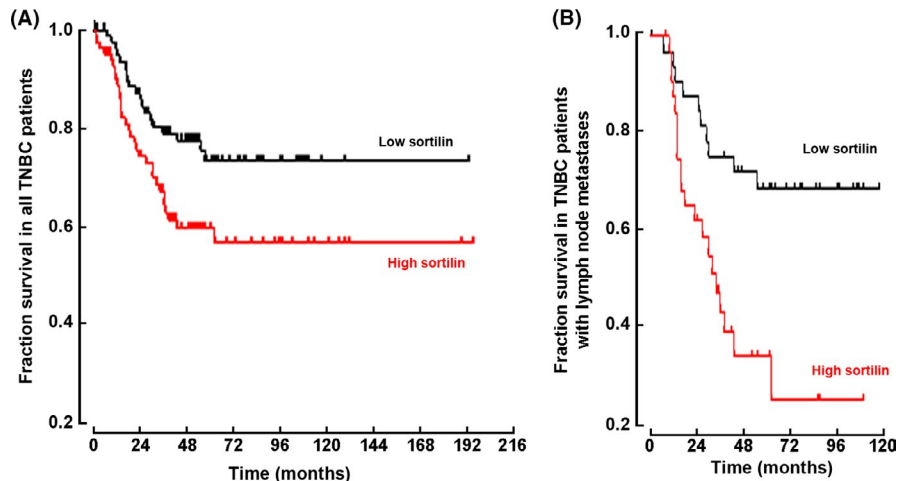


**FIGURE 3** SORT1-mediated TH19P01 peptide uptake in MDA-MB-231 cells. Transient *SORT1* gene silencing was performed as described in the Methods section and confirmed by (A) Western blotting and (B) densitometric analysis of *SORT1* protein expression. Experiment was performed in triplicate and the densitometric data analyzed using a *t*-test. (C) The binding (left panel) or uptake (right panel) of 200 nM Alexa<sup>488</sup>-labeled TH19P01 was performed in control (siScrambled) or *SORT1*-deficient (siSORT1) MDA-MB-231 cancer cells. The levels of fluorescence in the two categories of cells were measured in triplicate (binding and uptake  $n = 3$ ). Affinity constants were extrapolated for (D) Alexa<sup>488</sup>-labeled TH19P01 cell surface binding (KD), and inhibitory constants ( $K_i$ ) for (E) uptake of 200 nM Alexa<sup>488</sup>-labeled TH19P01 performed in the presence of increasing TH1902, TH19P01, or Neurotensin as indicated. Data are represented as mean  $\pm$  SD and statistical analysis was performed using Student's unpaired *t* test (\* $P < .05$ , \*\* $P < .01$ )

### 3.4 | Chemical synthesis strategy for TH1902 conjugation

The strategy for the conjugation of docetaxel to TH19P01 is described in the Methods section and schematized (Figure 5). In this

strategy, a cleavable ester linker was used for conjugation of the docetaxel to the TH19P01. On the TH19P01 peptide, the N-terminal site was first blocked by acetylation and the two other conjugation sites were saturated with docetaxel (Figure 5A). This led to the generation of a peptide-drug conjugate with two molecules of docetaxel

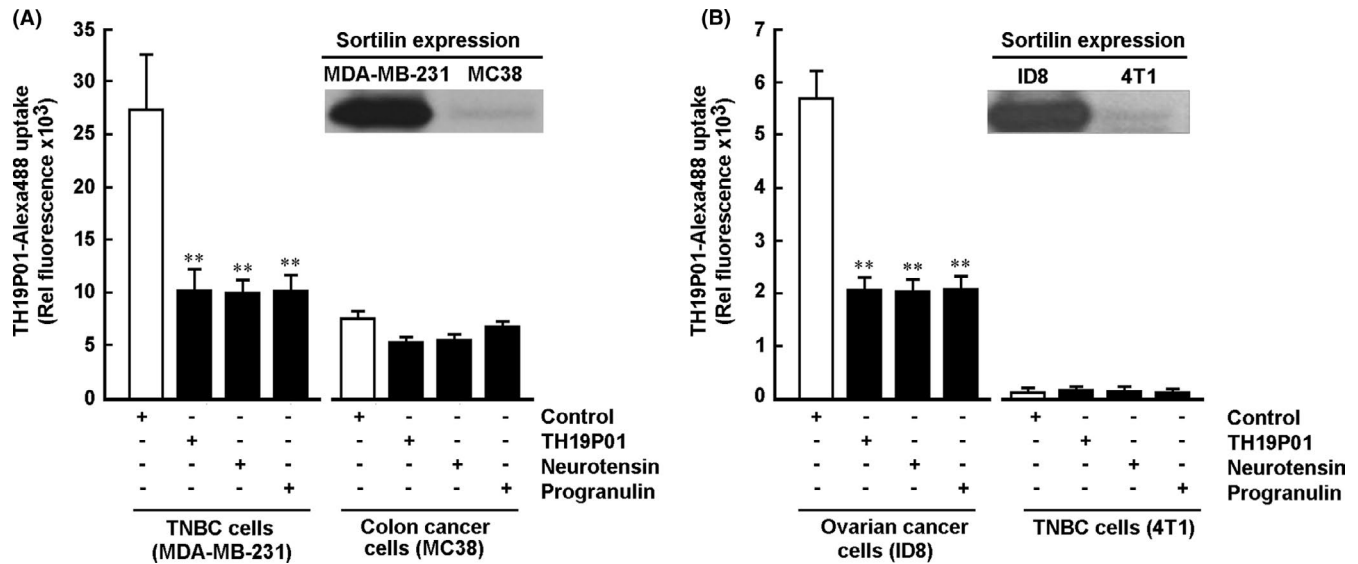


**FIGURE 4** Assessment of SORT1 expression requirement for TH19P01 peptide uptake in different cancer cell models. The uptake of 200 nM Alexa<sup>488</sup>-labeled TH19P01 was evaluated in (A) human TNBC cells (MDA-MB-231), human colon cancer cells (MC38), and (B) murine ovarian cancer cells (ID8), and murine TNBC cells (4T1). This was performed in the absence (white bar) or presence (black bars) of excess unlabeled TH19P01 (50  $\mu$ M), Neurotensin (NT, 10  $\mu$ M) or Progranulin (PGRN, 1.5 nM). Data are represented as mean  $\pm$  SD (ID8,  $n = 3$ ; 4T1,  $n = 5$ ; MDA-MB-231 and MC38,  $n = 2$ ) and statistical analysis was performed using Dunnet's test (\* $P < .05$ , \*\* $P < .01$ ). Inserts are representative immunodetections of Sortilin in whole cell lysates from each of the cell models tested

per peptide molecule (TH1902). The conjugation product was analyzed by UPLC and by mass spectrometry (MALDI-TOF). UPLC/MS analysis indicated that the purity of TH1902 (peak 1) was more than 95% (Figure 5B) and that the TH1902 conjugate had an estimated  $m/z$  mass of 1852.91 (charge +2) or 1235.62 (charge +3) (Figure 5C), corresponding to a molecular weight of 3704 g/mol for the TH1902 conjugate as compared to 807.9 g/mol for free docetaxel.

### 3.5 | *In vitro* anticancer properties of TH1902

To determine whether docetaxel or TH1902 inhibited TNBC cell proliferation, MTT assays were performed in MDA-MB-231 and HCC-70 cells exposed to various concentrations of TH19P01, docetaxel or TH1902. Inhibition of MDA-MB-231 cell proliferation was effectively triggered by both docetaxel and TH1902 compounds in a concentration-dependent manner whereas TH19P01 had no effect at the concentrations tested (Figure 6A). The IC<sub>50</sub> value of TH1902 was found to be comparable to that of docetaxel at low nM concentrations in both MDA-MB-231 and HCC-70 cells (Figure 6B), which supports the rationale that conjugated docetaxel can indeed be released from TH1902 once internalized and exert its antiproliferative effect inside the targeted cancer cells. The effect of TH1902 on MDA-MB-231 cell-cycle arrest was also tested (Figure 6C). The results show that more than 70% of treated cells were arrested in the G2/M phase of the cell cycle in comparison to vehicle-treated control cells where ~14% of the cells remained in the G2/M phase (Figure 6D). While TH19P01 appears to be an inert peptide with no *in vitro* antiproliferative effects, these data confirm both the growth inhibitory effect of TH1902 and, more importantly, that the

docetaxel anticancer potency was unaffected by its conjugation to the TH19P01 peptide.

### 3.6 | TH1902 triggers cell death in a TNBC-derived MDA-MB-231 cell model

The impact of docetaxel and TH1902 on MDA-MB-231 cellular morphology was evaluated and visualized by light microscopy. A drastic change in cell shape was observed in both docetaxel- and TH1902-treated cells when compared to control cells (Figure 7A). As already reported for docetaxel-treated human renal clear cell carcinoma,<sup>43</sup> MDA-MB-231 cells treated with docetaxel appeared more contracted than control cells. Interestingly, TH1902-treated cell morphology appeared even smaller, less flattened, and presented greater inter-cell spacing in comparison to those treated with free docetaxel (Figure 7A). This observation confirms the enhanced cytotoxic effect of TH1902 when compared to docetaxel. Docetaxel is further believed to exert its cytotoxic effects through both cell cycle regulation and apoptosis induction.<sup>44</sup> MDA-MB-231 cells were therefore treated for 5 or 24 hours with various concentrations of either docetaxel or TH1902, followed by AnnexinV/PI staining. TH1902 increased MDA-MB-231 cell apoptosis in a dose-dependent manner (Figure 7B, black bars) when compared to docetaxel treatment (Figure 7B, white bars). Less than 1% apoptotic cells were measured when cells were treated with 50  $\mu$ M TH19P01 for 24 hours (data not shown). Overall, this suggests that, even within such a short time frame, receptor-mediated events account for the increased effects of TH1902. Finally, to confirm the role of SORT1 in TH1902 internalization





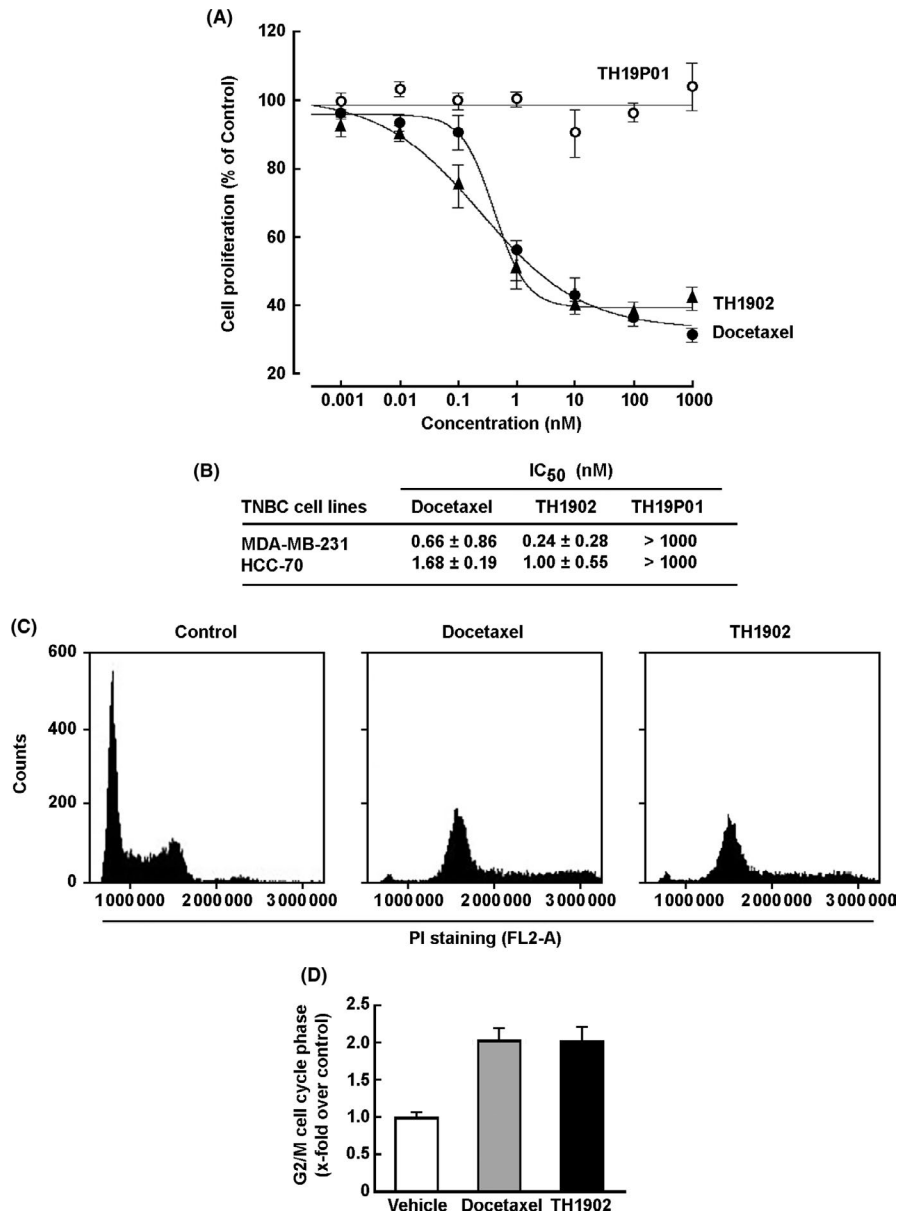


**FIGURE 6** *In vitro* anticancer properties of TH1902. A, A representative plot of the *in vitro* antiproliferative activities of TH19P01, docetaxel and TH1902 was determined from MTT assays in MDA-MB-231 as described in the Methods section. B, IC<sub>50</sub> values were calculated using a log[inhibitor] vs response-constant slope equation with GraphPad Prism software. IC<sub>50</sub> values are presented as mean ± SD from human TNBC-derived MDA-MB-231 and HCC-70 cells. All assays were performed in quadruplicate ( $n = 3$  experiments, except for TH1902  $n = 4$ ). C, A representative cell-cycle phase distribution of MDA-MB-231 cells was determined based on cellular DNA content (propidium iodide staining) after a 2 h treatment with 4  $\mu$ M docetaxel or 2  $\mu$ M TH1902 then followed by a 22 h incubation in complete media alone. D, Quantification of MDA-MB-231 G2/M cell cycle arrest following docetaxel or TH1902 treatment. Data represent mean ± SD ( $n = 4$ )

### 3.7 | Mechanism of TH1902-mediated apoptosis and antimigratory effect

Taxanes, including paclitaxel and docetaxel, are microtubule-stabilizing agents which alter microtubule dynamics and consequently induce mitotic arrest in cancer cells.<sup>43</sup> To assess whether TH1902 conserved this property, a tubulin immunofluorescent staining assay was performed in control, docetaxel-, and TH1902-treated MDA-MB-231 cells. Similar to docetaxel, TH1902 induced a marked microtubule bundling (Figure 8A). The expression levels of the anti-apoptotic Bcl-xL were next analyzed by Western blotting in MDA-MB-231 cells to investigate the molecular mechanisms by which TH1902 exerts its anticancer activity. The expression of Bcl-xL was assessed by immunoblotting (Figure 8B) and was found to be more reduced in TH1902-treated cells than in docetaxel-treated

cells (Figure 8C). This differential effect confirms that TH1902 acts through a distinct mechanism of action than the unconjugated docetaxel drug in apoptotic cell death-inducing events.

To further link the importance of microtubule perturbation and to compare the impacts of docetaxel and TH1902 on MDA-MB-231 breast cancer cell migration, transient silencing of SORT1 was performed, followed by a 2-hour treatment with docetaxel (Figure 8D) or TH1902 (Figure 8E). The results show that both docetaxel and TH1902 inhibit cell migration, but that this reduction was significantly prevented only in TH1902-treated cells where SORT1 was repressed (red arrow in Figure 8E). These results emphasize distinct mechanisms of action for TH1902 and docetaxel, and further support a SORT1 receptor-mediated internalization mechanism for TH1902 in contrast to that of passive diffusion for docetaxel.

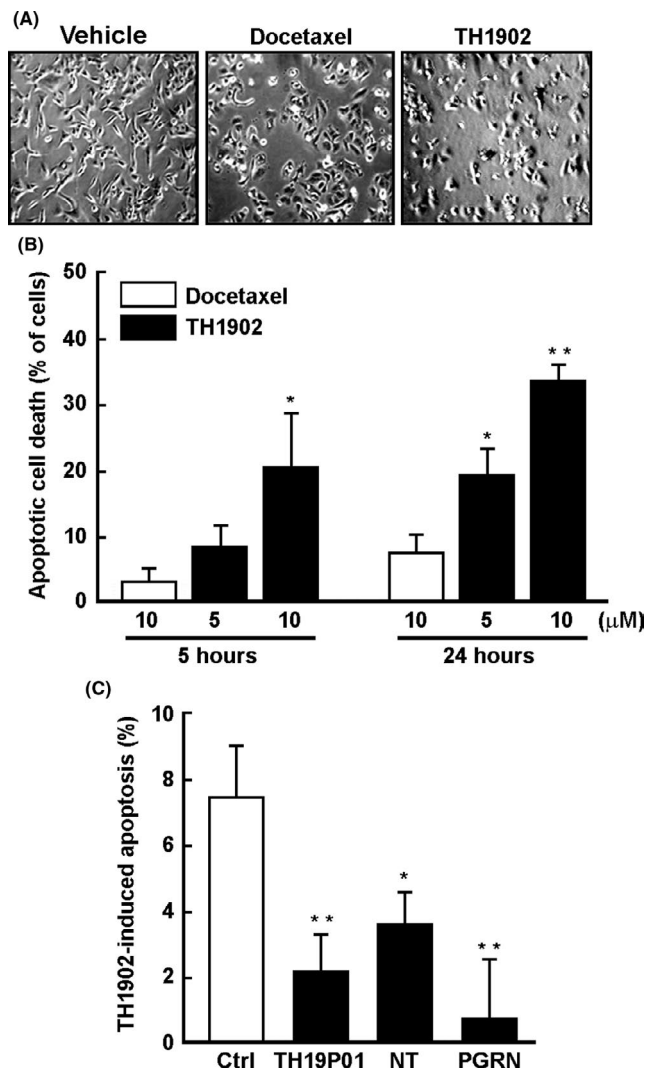


**FIGURE 7** Cell death induction by docetaxel and TH1902 in MDA-MB-231 cells. A, MDA-MB-231 cells were treated with vehicle, 10  $\mu\text{M}$  docetaxel or 5  $\mu\text{M}$  TH1902 for 24 h and cellular morphology was examined under a light microscope. B, MDA-MB-231 cells were treated for 5 or 24 h with 10  $\mu\text{M}$  docetaxel (white bars), or with 5–10  $\mu\text{M}$  TH1902 (black bars). Cells were then harvested and the extent of apoptotic cell death determined by flow cytometry following staining with AnnexinV-FITC and propidium iodide. Data are represented as mean  $\pm$  SEM ( $n = 3$ , except for the 5  $\mu\text{M}$  data where  $n = 7$ ). C, TH1902-mediated apoptosis in MDA-MB-231 cells was competed by an excess of free TH19P01 peptide (50  $\mu\text{M}$ ) or one of the SORT1 ligands neurotensin (NT, 10  $\mu\text{M}$ ) or progranulin (PGRN, 1 nM). Following 5 h of incubation, cells were stained with AnnexinV-FITC/PI. All data are represented as mean  $\pm$  SD ( $n = 3$ ) and statistical analysis was performed using one-way ANOVA with Dunnett's multiple comparison test (B and C) (\* $P < .05$ , \*\* $P < .01$ )

### 3.8 | Intraperitoneal administration of TH1902 inhibits tumor growth in a TNBC xenograft model

The *in vivo* efficacy of TH1902 and docetaxel against a TNBC xenograft model was next investigated *in vivo*. Thus, nude mice were implanted in the right flank with MDA-MB-231-luc cancer cells, and

luminescence was measured to monitor tumor growth. Mice were treated with intraperitoneal injections of either docetaxel at the MTD of 15 mg/kg/wk, or with TH1902 at the maximal injectable dose of 50 mg/kg/wk, both for five cycles of treatment. Unlike the vehicle-treated control group, where the average tumor luminescence increased over time, a significant decline in luminescence intensity was observed, starting at day 5 in the TH1902-treated group (Figure 9A). The level of luminescence intensity was also significantly lower in the free docetaxel-treated group, when compared to that in the vehicle-treated control group, but remained higher than that for the TH1902-treated group (Figure 9B). Interestingly, tumor relapse was observed in the docetaxel-treated group beginning at day 46, whereas a sustained decrease of tumor volume was maintained in the TH1902-treated group until day 74, at which time point a complete disappearance of the tumor was achieved (Figure 9A). Representative images of luminescence are shown for vehicle-, docetaxel-, or TH1902-treated mice at day 14 (Figure 9B, upper panels) when the control group reached the tumor volume endpoint and at day 74 post-treatment at the end of the experiment (Figure 9B, lower panels). Quantification of the residual tumor burden at days 14 and 74 after docetaxel or TH1902 treatment was performed, and the analysis confirmed a much better *in vivo* TH1902 efficacy profile than was seen with unconjugated docetaxel (Figure 9C). Given the lack of apoptotic or antiproliferative effects of TH19P01, no rationale supports its further assessment *in vivo*. As TH1902 is considered a new chemical entity, its best control condition therefore is the unconjugated docetaxel molecule itself. Body weight of mice on intraperitoneal administration of either docetaxel or TH1902 remained within endpoint limits ( $\sim 20\%$ , data not shown).

### 3.9 | Intravenous administration of TH1902 inhibits tumor growth in a TNBC xenograft model

The use of intravenous administration of TH1902 was next investigated in the TNBC-derived MDA-MB-231 xenograft model. Mice subjected to docetaxel treatment were administered with three intravenous injections at 15 mg/kg/wk (MTD), whereas those treated with TH1902 received five injections of an equivalent dose of docetaxel at 35 mg/kg/wk. Similar to what was seen with the intraperitoneal administration protocol, a sustained decrease in tumor size was observed following intravenous administration of TH1902 until day 70, whereas a restart of tumor growth was observed at day 50 for the docetaxel-treated mice (Figure 10A). When lower doses, equivalent to the quarter of the MTD, were used of docetaxel (3.75 mg/kg) and TH1902 (8.75 mg/kg) (Figure 10B), tumor growth as assessed by luminescence intensity was unaffected by intravenous administration of docetaxel, whereas it was significantly inhibited in the TH1902-treated group (Figure 10C). This was further confirmed through the measurement of the tumor burden luminescence where TH1902 reduced it significantly in comparison to vehicle- or docetaxel-treated groups (Figure 10D). Interestingly, body weight changes remained within endpoint limits in mice on intravenous administration of

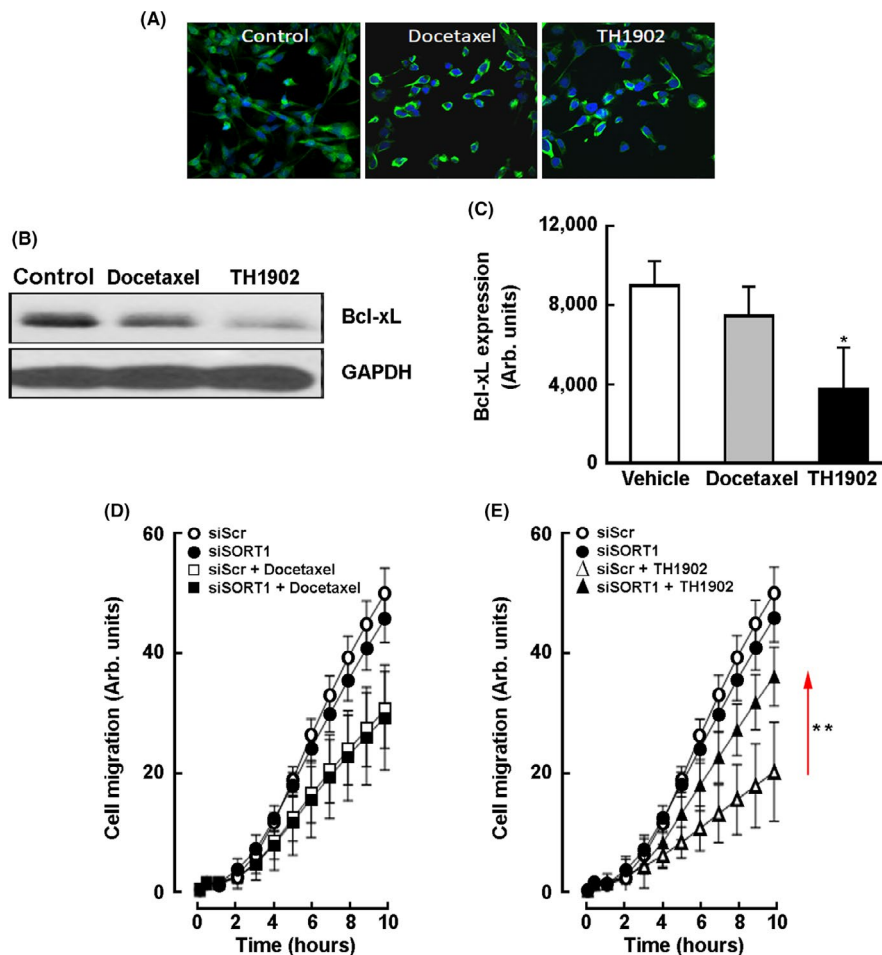


**FIGURE 8** Effect of TH1902 on MDA-MB-231 microtubules and cell migration. A, MDA-MB-231 cells were treated with vehicle (DMSO), 2  $\mu$ M docetaxel or 1  $\mu$ M TH1902 for 24 h, fixed and immunostained with anti- $\alpha$ -tubulin antibody, DNA stained with DAPI, and then imaged using confocal fluorescence microscopy. Representative pictures from each condition are displayed. (B) Representative immunoblot showing the protein expression level of Bcl-xL in MDA-MB-231 cells after treatment with docetaxel (100 nM) or TH1902 (50 nM) for 48 h. GAPDH was used as a loading control. Data are representative of three independent experiments. (C) Quantification of Bcl-xL was performed by scanning densitometry. Data represent mean  $\pm$  SD of arbitrary units and statistical analysis was performed using one-way ANOVA with Dunnet's test compared to control, (\* $P$  < .05,  $n$  = 3). The impact of (D) docetaxel and (E) TH1902 on MDA-MB-231 cell migration was evaluated with and without siRNA-mediated silencing of *SORT1*. Transfected cells were pretreated for 2 h with TH1902 (1  $\mu$ M) or docetaxel (2  $\mu$ M). Cells were harvested and their migratory potential assessed in real time as described in the Methods section. Data of normalized arbitrary units are represented as mean  $\pm$  SD of two experiments performed in duplicate. Statistical analysis of data at 10 h was performed using one-way ANOVA with Dunnet's multiple comparisons test (\*\* $P$  < .01)

either docetaxel or TH1902 (data not shown). Similar conclusions were reached on testing another TNBC-derived HCC-70 xenograft model (Figure 11). In fact, administration of TH1902 at 8.75 mg/kg/wk led to a 93% inhibition of HCC-70 tumor growth as compared to 24% for docetaxel alone at an equivalent dose.

### 3.10 | Absence of hematotoxicity of TH1902 in mice

Potential hematotoxicity on intravenous administrations of docetaxel and TH1902 to immunodeficient mice was next assessed. Interestingly, the neutrophil count decreased significantly in docetaxel-treated mice at MTD after three cycles of treatment, whereas neutrophil levels remained within normal limits in TH1902-treated mice at an equivalent dose of docetaxel (Figure 12A), and

this remained even after six TH1902 injections. This crucial observation suggests that TH1902 would have a better hematological toxicity profile than the native docetaxel molecule. Body weight was also monitored during these treatments. The results show that administration of docetaxel induced significant body weight loss (>10%) in some mice after only three treatments (Figure 12B). In contrast, animal body weight was unaffected by the administration of up to six TH1902 treatments.

### 3.11 | Preliminary pharmacokinetics of TH1902 in mice

Preliminary pharmacokinetics for TH1902 was also evaluated in normal CD-1 mice. TH1902 plasma concentrations were measured by

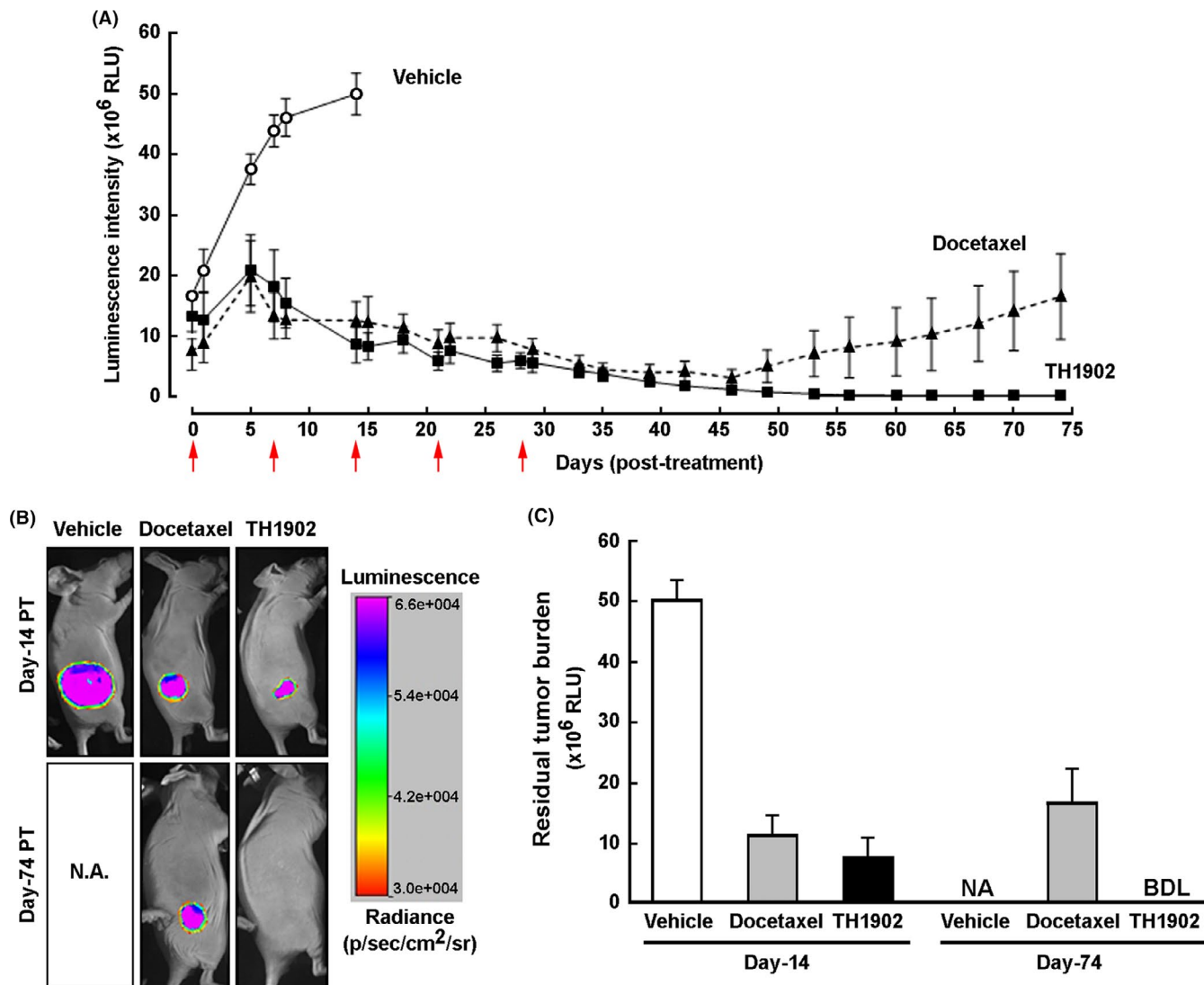


**FIGURE 9** Comparative efficacy of docetaxel and TH1902 on MDA-MB-231 xenograft tumor growth. A, Nude mice were subcutaneously implanted with MDA-MB-231-Luc cells and then treated with vehicle, docetaxel or TH1902 as described in the Methods section. Intraperitoneal (i.p.) treatments are indicated by red arrows. B, Representative bioluminescence images were taken at 14 and 74 days post-implantation of MDA-MB-231-Luc cells into the mice. In the color bar, violet and red indicate the highest and lowest intensity of exposure, respectively. Results are expressed in terms of tumor luminescence intensity at day 0 post-treatment for each mouse. C, Tumor burden was expressed as net luminescence intensity at days 14 and 74 post-treatment. Data are represented as mean  $\pm$  SEM (six mice/group). At day 74, all control mice were already sacrificed. Therefore, NA in this panel indicates that bioluminescence is not available (NA) for this group, whereas the bioluminescence in TH1902-treated mice was below detectable levels (BDL)

UPLC/MS after a single i.v. bolus injection at 50 mg/kg (Figure 13, closed circles). The distribution and elimination half-life ( $t_{1/2}$ ) were estimated at 0.46 and 1.44 hours, respectively. Plasma concentrations of released docetaxel (Figure 13, black squares) suggest that most docetaxel remained associated with the peptide over the time course analyzed. Pharmacokinetic measures of docetaxel exposure ( $C_{max}$  and AUC) showed that free docetaxel exposure was approximately 37-fold lower than that of TH1902-associated docetaxel in plasma (AUC = 569  $\mu\text{mol/L h}$  for TH1902 versus 15.5  $\mu\text{mol/L h}$  for free docetaxel, and  $C_{max}$  = 388  $\mu\text{mol/L}$  for TH1902 versus 7  $\mu\text{mol/L}$  for free docetaxel). Low levels of free docetaxel in mouse plasma may in part explain the absence of neutropenia in mice and account for the higher safety of TH1902.

#### 4 | DISCUSSION

Numerous studies have revealed the complex molecular signature characterizing TNBC, clearly establishing their intra- and inter-tumor heterogeneity.<sup>45</sup> Consequently, these cancers were redefined into phenotypic subtypes which remain among the most difficult to treat, relying on a standard of care chemotherapy using cytotoxic agents. Unfortunately, chemotherapy is also known for its limited tumor selectivity and, consequently, is responsible for several adverse treatment side effects and for the development of a drug resistance phenotype. Several attempts at designing targeted strategies such as using the EGFR monoclonal antibody, failed to provide an appropriately improved outcome.<sup>46,47</sup> The design of novel anticancer



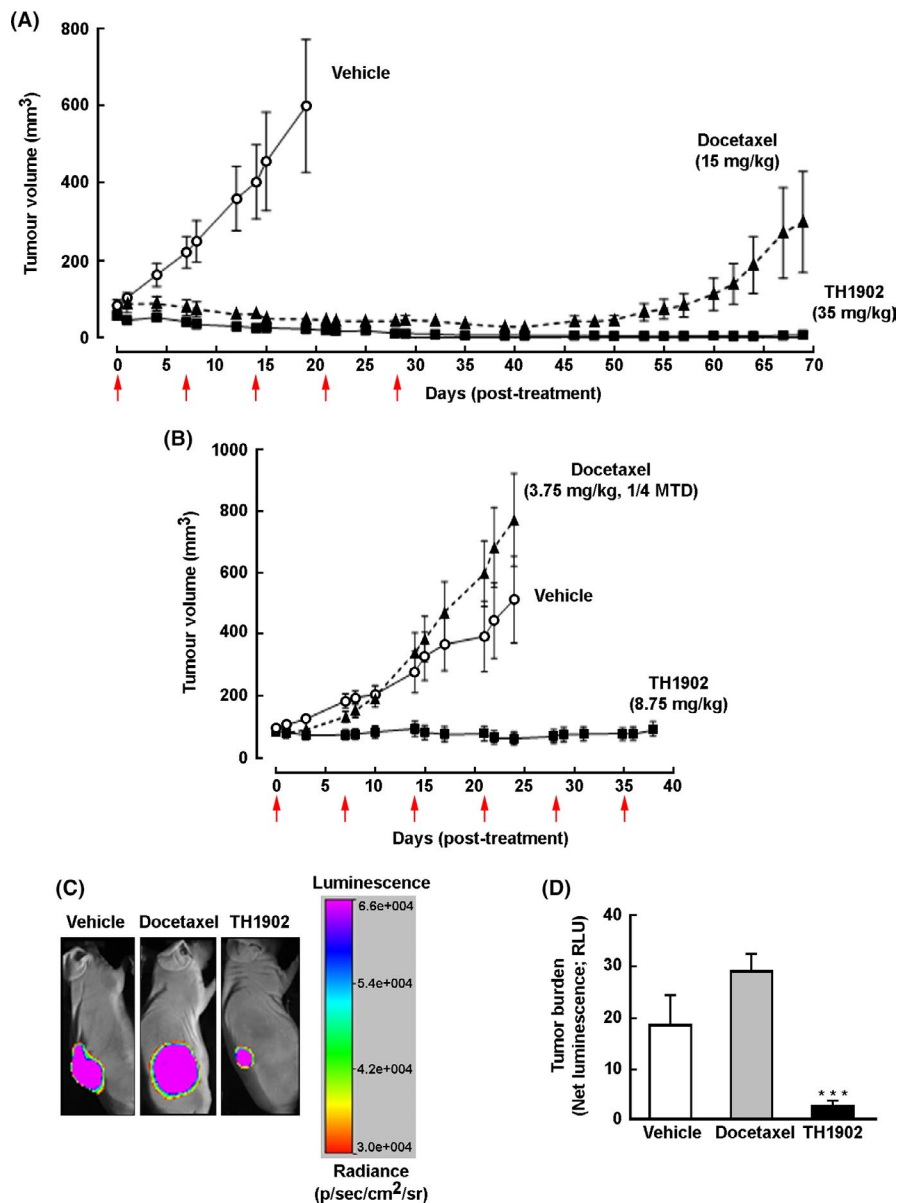


**FIGURE 10** Intravenous administration of TH1902 inhibits tumor growth in a MDA-MB-231 TNBC xenograft model. A, Nude mice were subcutaneously implanted with TNBC-derived MDA-MB-231 cells and then treated with vehicle or with either docetaxel (15 mg/kg, three cycles) or TH1902 (35 mg/kg, five cycles) as described in the Methods section. Intravenous (i.v.) treatments are indicated by red arrows. B, Tumor volume progression measured as above for vehicle, docetaxel (3.75 mg/kg), or TH1902 (8.75 mg/kg) treatments. C, Representative bioluminescence images were taken at day 27 post-implantation of MDA-MB-231-Luc cells into the mice. In the color bar, violet and red indicate the highest and lowest intensity of exposure, respectively. D, Tumor burden was expressed as net luminescence intensity at day 27. Data are represented as mean  $\pm$  SEM and statistical analysis was performed using one-way ANOVA with Dunnett's test compared to control (A,  $n = 5$  mice/group; B-D,  $n = 6$  mice/group, \*\*\* $P < .001$ )

drugs and more efficient targeted therapies are therefore required to increase the therapeutic outcome of TNBC patients.<sup>48,49</sup>

In this study, a new docetaxel-TH19P01 peptide drug conjugate (TH1902) was created. Its *in vitro* receptor-mediated internalization mechanism was characterized using a well-documented TNBC cell model, whereas TH1902 *in vivo* anticancer efficacy was studied in two TNBC xenograft models. This peptide-drug conjugation platform therefore allows for increased breast cancer cell targeting and enhanced penetration of docetaxel in SORT1-positive TNBC. The molecular rationale for our anticancer therapy further relies on the numerous benefits our conjugation platform offers over current conjugates that involve antibodies or proteins. Advantages include smaller size conjugates, which allows for greater plasma membrane penetration with better tissue specificity and cell selectivity, leading to increased intracellular cytotoxic activity and resulting in better safety.<sup>50</sup> Additionally, the efficient use of therapeutic peptides, as specific receptor targeting ligands, benefits from their inexpensive,

rapid synthesis, easier modification, and increased affinity compared to what is seen with antibodies.<sup>51-55</sup>

TH1902 pharmacological anticancer properties in mechanisms involving cell apoptosis, proliferation, migration, peptide internalization, and impact on cytoskeleton dynamics were further revealed in this study. TH1902 was able to induce apoptotic cell death faster than free docetaxel. TH1902 also blocked cell cycle progression in the G2/M phase confirming that, once internalized, docetaxel is effectively released from the conjugate.<sup>56-58</sup> The rapid cytotoxic effect of TH1902 (<5 hours) also further supports the concept of a significant ligand internalization process regulated by SORT1.

Studies on breast cancer cells demonstrate the association of their intrinsic or acquired resistance phenotype with dysfunctional apoptosis signalling.<sup>59,60</sup> Overexpression of Bcl-2 and Bcl-xL has been observed in several solid cancers, including colorectal, prostate, and breast cancer.<sup>61-63</sup> Downregulation of Bcl-xL protein expression by antisense oligodeoxynucleotides in various tumor cell lines

**FIGURE 11** Intravenous administration of TH1902 inhibits tumor growth in a HCC-70 TNBC xenograft model. A, Nude mice were subcutaneously implanted with TNBC-derived HCC-70 cells and then treated with vehicle or with either docetaxel (3.75 mg/kg, 1/4 MTD) or TH1902 (8.75 mg/kg) as described in the Methods section. Intravenous treatments are indicated by red arrows. B, Tumor volume progression measured as above for vehicle, docetaxel (3.75 mg/kg), or TH1902 (8.75 mg/kg) treatments. Data are represented as mean ± SEM and statistical analysis was performed using one-way ANOVA with Dunnett's test compared to control (vehicle,  $n = 7$ ; docetaxel and TH1902,  $n = 6$  mice/group;  $**P < .01$ )

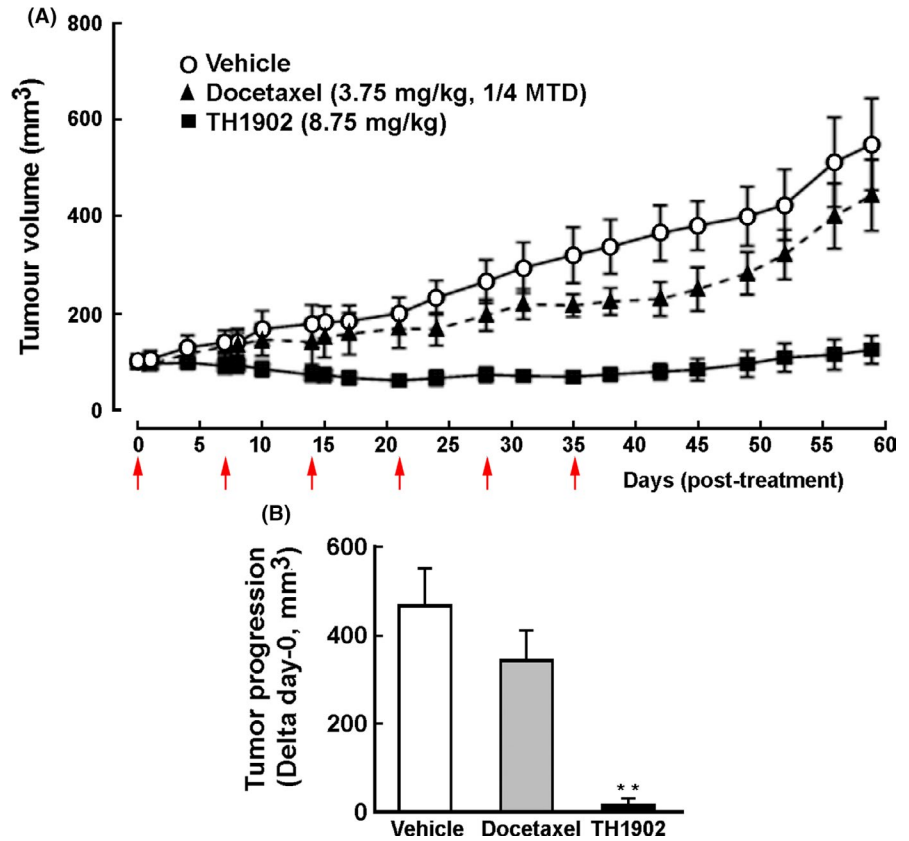
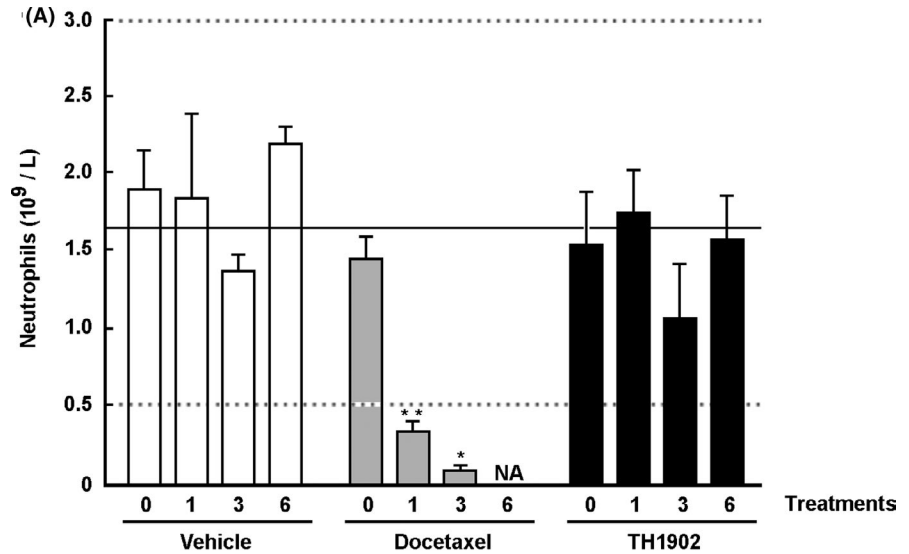


**FIGURE 12** Absence of hematotoxicity of TH1902 in mice. A, Athymic nude mice were treated with docetaxel at MTD (15 mg/kg/wk, three cycles) or with an equivalent dose of TH1902 (up to six cycles). Blood was collected 4 days before the initiation of treatments and 4 days after the first, third and sixth treatments to assess the drug effects on neutrophil blood cell counts. Neutrophils count was not available (NA) for mice treated with docetaxel since treatment was stopped after three cycles. Data are represented as mean ± SEM and statistical analysis was performed using a t-test against initial values observed at treatment 0 ( $n = 5$  mice for treatments 0, 1 and 6;  $n = 2$  mice for treatment 3;  $*P < .05$ ,  $**P < .01$ ). B, Body weight of mice was monitored with relation to the treatments. The number of mice with variations in body weight (>5% and 10%) after three or six treatments is presented ( $n = 5$  mice/group)



**(B)**

		Docetaxel	TH1902
Number of treatments	Weight loss	Number of mice	Number of mice
3	>5%	3 / 5	0 / 5
	>10%	2 / 5	0 / 5
6	>5%	N.A.	1 / 5
	>10%	N.A.	0 / 5

resulted in activation of apoptosis, as well as decreased cellular proliferation and increased sensitivity to cytotoxic chemotherapeutic agents.<sup>64,65</sup> Data from this study support the rapid and preferential

receptor-mediated induction of apoptosis by TH1902 through, in part, the reduction of the anti-apoptotic Bcl-xL expression. This is of considerable importance, as increased expression levels or

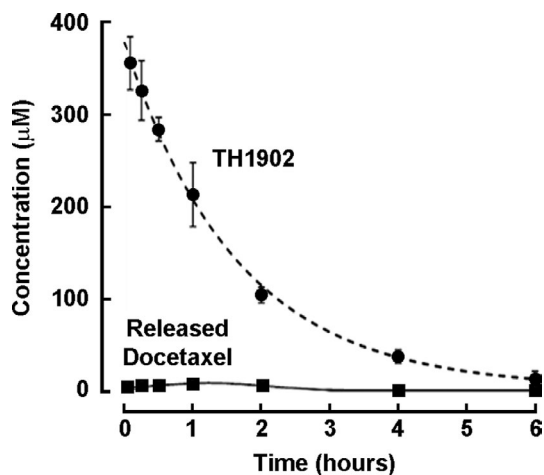


**FIGURE 13** Preliminary pharmacokinetics of TH1902 in mice. Normal CD-1 mice were injected i.v. with TH1902 (50 mg/kg). Plasma samples for pharmacokinetic characterization were collected at the indicated times after i.v. bolus injection of TH1902. TH1902 and docetaxel concentrations were determined by UPLC/MS as described in the Methods section. Both TH1902 and free docetaxel plasmatic concentrations were plotted as a function of time.  $C_{max}$ , termination half-life and AUC were estimated using the PK solution software. Data are represented as mean  $\pm$  SEM (n = 3 to 6 mice per time point)

post-translational modifications of Bcl-2 family members, including Bcl-xL, have been associated with resistance to taxanes.<sup>66,67</sup> This is an interesting finding since TNBC-derived MDA-MB-231 cells are known to be resistant to docetaxel-induced apoptosis in part due to high Bcl-xL levels,<sup>68-70</sup> and further establishes that TH1902-mediated apoptotic cell death occurs through its SORT1-mediated internalization. Overall, TH1902 treatment therefore appears to circumvent the anti-apoptotic functions believed, in part, to be associated with chemoresistance in TNBC cells.

Impairment of mitotic progression coupled to inhibition of cell proliferation and of signaling pathways are critical cellular processes known to be targeted by docetaxel and which are partly explained by its intracellular action on microtubule dynamics.<sup>71</sup> Given the observed tubulin perturbation, this study confirms that, even on TH19P01 peptide conjugation, docetaxel, once released from TH1902, retained a similar intracellular mechanism of action as that of free docetaxel by interfering with the dynamics of microtubules. Interestingly, evidence suggests that the TH19P01 peptide required cell surface clathrin-coated vesicles to be internalized and to reach the lysosomal compartment where docetaxel could be released from TH1902 by esterases and the peptide cleaved by proteases.<sup>39</sup> This again supports TH1902 as a new entity requiring an internalization mechanism distinct from that of free docetaxel.

The molecular rationale supporting SORT1 as a therapeutic target is strengthened by its highly expressed levels on the cell surface of multiple tumor types including ovarian cancer, prostate cancer, skin cancer, and breast cancer.<sup>33-37</sup> In this study, high expression levels of SORT1 were observed in tumor biopsies and in ILNC. In

addition, *in silico* predictive analysis of TNBC patients using Kaplan-Meier software confirmed that patients with high SORT1 gene expression had a poorer prognosis than patients with low SORT1 gene expression, particularly in TNBC patients with lymph node metastases. This observation is further reinforced by a study conducted on 318 breast cancer patients where SORT1 was upregulated in 79% of IDC and 59% of the TNBC subtypes.<sup>34</sup> Recently, anti-PD-L1 antibodies have demonstrated some promising clinical efficacy against diverse tumor types where early findings revealed a durable clinical response in only a small (10%-13%) fraction of metastatic TNBC patients treated with antagonists for the PD-1/PD-L1 pathway.<sup>72,73</sup> When compared to PD-L1, which was found to be upregulated in only 19% of this breast cancer subtype,<sup>74</sup> SORT1 expression was threefold higher in TNBC, which provides an additional advantage in exploiting SORT1 receptor-mediated chemotherapy for this difficult-to-treat disease. Accordingly, our results indicate that SORT1-mediated chemotherapy may be envisioned as a novel, personalized, targeted approach for the treatment of patients with SORT1-positive TNBC. Finally, the present *in vivo* data demonstrate that both intraperitoneal and intravenous TH1902 administrations are well tolerated and lead to better tumor growth inhibition and an absence of tumor relapse after repeated treatments in the two xenograft models of mice tested.

Taken together, TH1902, by targeting SORT1, showed a better efficacy when administered at the equivalent MTD for docetaxel and even at a quarter of this dose. Importantly, and within the treatment modalities used, neither neutropenia nor body weight loss, two of the major adverse toxic effects associated with docetaxel, were observed after TH1902 treatments. The efficacy data and the absence of major adverse effects indicate that TH1902 could have a higher therapeutic window than docetaxel. This study therefore demonstrates that efficient SORT1 receptor-mediated chemotherapy could be developed through this versatile anticancer drug conjugation platform to TH19P01 peptide. Such a platform flexibility allows personalized medicine to be envisioned by targeting TNBC patients with SORT1-positive primary or metastatic tumors.

## ACKNOWLEDGMENTS

BA holds an institutional Research Chair in Cancer Prevention and Treatment.

## DISCLOSURE

MD, AL, RB and BA were scientific founders of Katana Biopharma. CM is senior vice president and chief medical officer at Theratechnologies.

## AUTHORS' CONTRIBUTIONS

CC, MD, BA and JCC carried out the design and coordination of the study. CC, MD, JCC and AL performed *in vitro* experiments. AL and SK performed *in vivo* experiments. AL performed the synthesis of TH1902. CC, MD, JCC, RB, CM, and BA analyzed the data and wrote the manuscript.

**ETHICAL APPROVAL AND CONSENT TO PARTICIPATE**

No ethics approval was required for this study as it did not involve patients or patient data.

**CONSENT FOR PUBLICATION**

All authors consent to publication.

**DATA AVAILABILITY STATEMENT**

All data generated or analysed during this study are included in this published article.

**ORCID**

Borhane Annabi  <https://orcid.org/0000-0002-5082-7183>

**REFERENCES**

- Sorlie T, Perou CM, Tibshirani R, et al. Gene expression patterns of breast carcinomas distinguish tumor subclasses with clinical implications. *Proc Natl Acad Sci USA*. 2001;98:10869-10874.
- Perou CM, Sorlie T, Eisen MB, et al. Molecular portraits of human breast tumours. *Nature*. 2000;406:747-752.
- Wolff AC, Hammond ME, Hicks DG, et al. Recommendations for human epidermal growth factor receptor 2 testing in breast cancer: American Society of Clinical Oncology/College of American Pathologists clinical practice guideline update. *J Clin Oncol*. 2013;31:3997-4013.
- Rakha EA, Reis-Filho JS, Ellis IO. Basal-like breast cancer: a critical review. *J Clin Oncol*. 2008;26:2568-2581.
- Parise CA, Caggiano V. Risk factors associated with the triple-negative breast cancer subtype within four race/ethnicities. *Breast Cancer Res Treat*. 2017;163:151-158.
- Newcomb PA, Storer BE, Longnecker MP, et al. Lactation and a reduced risk of premenopausal breast cancer. *N Engl J Med*. 1994;330:81-87.
- McTiernan A, Thomas DB. Evidence for a protective effect of lactation on risk of breast cancer in young women. Results from a case-control study. *Am J Epidemiol*. 1986;124:353-358.
- Lowe CR, MacMahon B. Breast cancer and reproduction. *Lancet*. 1970;2:1137.
- Mirra AP, Cole P, MacMahon B. Breast cancer in an area of high parity: Sao Paulo, Brazil. *Cancer Res*. 1971;31:77-83.
- Wetterskog D, Lopez-Garcia MA, Lambros MB, et al. Adenoid cystic carcinomas constitute a genomically distinct subgroup of triple-negative and basal-like breast cancers. *J Pathol*. 2012;226:84-96.
- Nunnery SE, Mayer IA, Balko JM. Triple-negative breast cancer: breast tumors with an identity crisis. *Cancer J*. 2021;27(1):2-7.
- Lehmann BD, Bauer JA, Chen X, et al. Identification of human triple-negative breast cancer subtypes and preclinical models for selection of targeted therapies. *J Clin Invest*. 2011;121:2750-2767.
- Lin NU, Vanderplas A, Hughes ME, et al. Clinicopathologic features, patterns of recurrence, and survival among women with triple-negative breast cancer in the National Comprehensive Cancer Network. *Cancer*. 2012;118:5463-5472.
- Anders CK, Carey LA. Biology, metastatic patterns, and treatment of patients with triple-negative breast cancer. *Clin Breast Cancer*. 2009;9(Suppl 2):S73-81.
- Cadoo KA, Fornier MN, Morris PG. Biological subtypes of breast cancer: current concepts and implications for recurrence patterns. *Q J Nucl Med Mol Imaging*. 2013;57:312-321.
- Guarneri V, Dieci MV, Conte P. Relapsed triple-negative breast cancer: challenges and treatment strategies. *Drugs*. 2013;73:1257-1265.
- Montagna E, Bagnardi V, Rotmensz N, et al. Breast cancer subtypes and outcome after local and regional relapse. *Ann Oncol*. 2012;23:324-331.
- de Ruijter TC, Veeck J, de Hoon JP, van Engeland M, Tjan-Heijnen VC. Characteristics of triple-negative breast cancer. *J Cancer Res Clin Oncol*. 2011;137:183-192.
- Chacon RD, Costanzo MV. Triple-negative breast cancer. *Breast Cancer Res*. 2010;12(Suppl 2):S3.
- Hudis CA, Gianni L. Triple-negative breast cancer: an unmet medical need. *Oncologist*. 2011;16(Suppl 1):1-11.
- Rapoport BL, Demetriou GS, Moodley SD, Benn CA. When and how do I use neoadjuvant chemotherapy for breast cancer? *Curr Treat Options Oncol*. 2014;15:86-98.
- Lehmann BD, Pietenpol JA, Tan AR. Triple-negative breast cancer: molecular subtypes and new targets for therapy. *Am Soc Clin Oncol Educ Book*. 2015;2015:e31-e39. [https://doi.org/10.14694/EdBook\\_AM.2015.35.e31](https://doi.org/10.14694/EdBook_AM.2015.35.e31)
- Nanda R, Chow LQ, Dees EC, et al. Pembrolizumab in patients with advanced triple-negative breast cancer: Phase Ib keynote-012 study. *J Clin Oncol*. 2016;34(21):2460-2467.
- Costa RLB, Gradishar WJ. Triple-negative breast cancer: current practice and future directions. *J Oncol Pract*. 2017;13(5):301-303.
- Han Y, Yu X, Li S, Tian Y, Liu C. New perspectives for resistance to PARP inhibitors in triple-negative breast cancer. *Front Oncol*. 2020;10:578095.
- Gupta GK, Collier AL, Lee D, et al. Perspectives on triple-negative breast cancer: current treatment strategies, unmet needs, and potential targets for future therapies. *Cancers (Basel)*. 2020;12(9):2392.
- Marcusson EG, Horzodovsky BF, Cereghino JL, Gharakhanian E, Emr SD. The sorting receptor for yeast vacuolar carboxypeptidase Y is encoded by the VPS10 gene. *Cell*. 1994;77:579-586.
- Vincent JP, Mazella J, Kitabgi P. Neurotensin and neurotensin receptors. *Trends Pharmacol Sci*. 1999;20:302-309.
- Mazella J, Zsuzer N, Navarro V, et al. The 100-kDa neurotensin receptor is gp95/sortilin, a non-G-protein-coupled receptor. *J Biol Chem*. 1998;273:6273-6276.
- Hu F, Padukkavidana T, Vaegter CB, et al. Sortilin-mediated endocytosis determines levels of the frontotemporal dementia protein, progranulin. *Neuron*. 2010;68:654-667.
- Carlo AS, Gustafsen C, Mastrobuoni G, et al. The pro-neurotrophin receptor sortilin is a major neuronal apolipoprotein E receptor for catabolism of amyloid-beta peptide in the brain. *J Neurosci*. 2013;33:358-370.
- Kjolby M, Nielsen MS, Petersen CM. Sortilin, encoded by the cardiovascular risk gene SORT1, and its suggested functions in cardiovascular disease. *Curr Atheroscler Rep*. 2015;17:496.
- Oh TJ, Ahn CH, Kim BR, et al. Circulating sortilin level as a potential biomarker for coronary atherosclerosis and diabetes mellitus. *Cardiovasc Diabetol*. 2017;16:92.
- Roselli S, Pundavela J, Demont Y, et al. Sortilin is associated with breast cancer aggressiveness and contributes to tumor cell adhesion and invasion. *Oncotarget*. 2015;6:10473-10486.
- Ghaemimanes F, Ahmadian G, Talebi S, et al. The effect of sortilin silencing on ovarian carcinoma cells. *Avicenna J Med Biotechnol*. 2014;6:169-177.
- Truzzi F, Marconi A, Lotti R, et al. Neurotrophins and their receptors stimulate melanoma cell proliferation and migration. *J Invest Dermatol*. 2008;128:2031-2040.
- Giorgi RR, Chile T, Bello AR, et al. Expression of neurotensin and its receptors in pituitary adenomas. *J Neuroendocrinol*. 2008;20:1052-1057.
- Gao F, Griffin N, Faulkner S, et al. The membrane protein sortilin can be targeted to inhibit pancreatic cancer cell invasion. *Am J Pathol*. 2020;190:1931-1942.

39. Demeule M, Currie JC, Larocque A, et al. Increasing potency of anticancer drugs through sortilin receptor-mediated cancer therapy: a new targeted approach for the treatment of ovarian cancer. *Cancer Res.* 2020;80(16 Supplement):1061.
40. Mosmann T. Rapid colorimetric assay for cellular growth and survival: application to proliferation and cytotoxicity assays. *J Immunol Methods.* 1983;65(1-2):55-63.
41. Schimpff RM, Gourmelin M, Scarcériaux V, Lhiaubet AM, Rostène W. Plasma neurotensin levels in humans: relation to hormone levels in diseases involving the hypothalamo-pituitary-thyroid axis. *Eur J Endocrinol.* 1995;133(5):534-538.
42. Meeter LH, Patzke H, Loewen G, et al. Progranulin levels in plasma and cerebrospinal fluid in granulin mutation carriers. *Dement Geriatr Cogn Dis Extra.* 2016;6(2):330-340.
43. Han TD, Shang DH, Tian Y. Docetaxel enhances apoptosis and G2/M cell cycle arrest by suppressing mitogen-activated protein kinase signaling in human renal clear cell carcinoma. *Genet Mol Res.* 2016;5:15.
44. Abal M, Andreu JM, Barasorain I. Taxanes: microtubule and centrosome targets, and cell cycle dependent mechanisms of action. *Curr Cancer Drug Targets.* 2003;3:193-203.
45. Wright N, Rida PCG, Aneja R. Tackling intra- and inter-tumor heterogeneity to combat triple negative breast cancer. *Front Biosci (Landmark Ed).* 2017;22:1549-1580.
46. Baselga J, Gomez P, Greil R, et al. Randomized phase II study of the anti-epidermal growth factor receptor monoclonal antibody cetuximab with cisplatin versus cisplatin alone in patients with metastatic triple-negative breast cancer. *J Clin Oncol.* 2013;31:2586-2592.
47. Carey LA, Rugo HS, Marcom PK, et al. TBCRC 001: randomized phase II study of cetuximab in combination with carboplatin in stage IV triple-negative breast cancer. *J Clin Oncol.* 2012;30:2615-2623.
48. Baudino TA. Targeted cancer therapy: the next generation of cancer treatment. *Curr Drug Discov Technol.* 2015;12:3-20.
49. Perez-Herrero E, Fernandez-Medarde A. Advanced targeted therapies in cancer: drug nanocarriers, the future of chemotherapy. *Eur J Pharm Biopharm.* 2015;93:52-79.
50. He R, Finan B, Mayer JP, DiMarchi RD. Peptide conjugates with small molecules designed to enhance efficacy and safety. *Molecules.* 2019;24(10):1855.
51. Boohaker RJ, Lee MW, Vishnubhotla P, Perez JM, Khaled AR. The use of therapeutic peptides to target and to kill cancer cells. *Curr Med Chem.* 2012;19:3794-3804.
52. Marqus S, Pirogova E, Piva TJ. Evaluation of the use of therapeutic peptides for cancer treatment. *J Biomed Sci.* 2017;24:21.
53. Adams GP, Schier R, McCall AM, et al. High affinity restricts the localization and tumor penetration of single-chain fv antibody molecules. *Cancer Res.* 2001;61:4750-4755.
54. Rudnick SI, Lou J, Shaller CC, et al. Influence of affinity and antigen internalization on the uptake and penetration of Anti-HER2 antibodies in solid tumors. *Cancer Res.* 2011;71:2250-2259.
55. Ali R, Sudhir RRaK. *New Peptide Based Therapeutic Approaches.* OMICS International; 2014.
56. Hernandez-Vargas H, Palacios J, Moreno-Bueno G. Molecular profiling of docetaxel cytotoxicity in breast cancer cells: uncoupling of aberrant mitosis and apoptosis. *Oncogene.* 2007;26:2902-2913.
57. Nehme A, Varadarajan P, Sellakumar G, et al. Modulation of docetaxel-induced apoptosis and cell cycle arrest by all- trans retinoic acid in prostate cancer cells. *Br J Cancer.* 2001;84:1571-1576.
58. Han TD, Shang DH, Tian Y. Docetaxel enhances apoptosis and G2/M cell cycle arrest by suppressing mitogen-activated protein kinase signaling in human renal clear cell carcinoma. *Genet Mol Res.* 2016;15.
59. Baguley BC. Multidrug resistance in cancer. *Methods Mol Biol.* 2010;596:1-14.
60. Mohammad RM, Muqbil I, Lowe L, et al. Broad targeting of resistance to apoptosis in cancer. *Semin Cancer Biol.* 2015;35:S78-S103.
61. Krajewski S, Krajewska M, Shabaik A, et al. Immunohistochemical analysis of in vivo patterns of Bcl-X expression. *Cancer Res.* 1994;54(21):5501-5507.
62. Hanada M, Aimé-Sempé C, Sato T, Reed JC. Structure-function analysis of Bcl-2 protein. Identification of conserved domains important for homodimerization with Bcl-2 and heterodimerization with Bax. *J Biol Chem.* 1995;270(20):11962-11969.
63. Olopade OI, Adeyanju MO, Safa AR, et al. Overexpression of BCL-x protein in primary breast cancer is associated with high tumor grade and nodal metastases. *Cancer J Sci Am.* 1997;3(4):230-237.
64. Simões-Wüst AP, Olie RA, Gautschi O, et al. Bcl-xl antisense treatment induces apoptosis in breast carcinoma cells. *Int J Cancer.* 2000;87(4):582-590.
65. Xu Z, Friess H, Solioz M, et al. Bcl-xL antisense oligonucleotides induce apoptosis and increase sensitivity of pancreatic cancer cells to gemcitabine. *Int J Cancer.* 2001;94:268-274.
66. Ibrado AM, Liu L, Bhalla K. Bcl-xL overexpression inhibits progression of molecular events leading to paclitaxel-induced apoptosis of human acute myeloid leukemia HL-60 cells. *Cancer Res.* 1997;57:1109-1115.
67. Wang Z, Goulet R 3rd, Stanton KJ, Sadaria M, Nakshatri H. Differential effect of anti-apoptotic genes Bcl-xL and c-FLIP on sensitivity of MCF-7 breast cancer cells to paclitaxel and docetaxel. *Anticancer Res.* 2005;25:2367-2379.
68. Lim LY, Vidnovic N, Ellisen LW, Leong CO. Mutant p53 mediates survival of breast cancer cells. *Br J Cancer.* 2009;101:1606-1612.
69. Morse DL, Gray H, Payne CM, Gillies RJ. Docetaxel induces cell death through mitotic catastrophe in human breast cancer cells. *Mol Cancer Ther.* 2005;4:1495-1504.
70. Nieves-Neira W, Pommier Y. Apoptotic response to camptothecin and 7-hydroxystaurosporine (UCN-01) in the 8 human breast cancer cell lines of the NCI Anticancer Drug Screen: multifactorial relationships with topoisomerase I, protein kinase C, Bcl-2, p53, MDM-2 and caspase pathways. *Int J Cancer.* 1999;82:396-404.
71. Ringel I, Horwitz SB. Studies with RP 56976 (taxotere): a semisynthetic analogue of taxol. *J Natl Cancer Inst.* 1991;83:288-291.
72. Shin DS, Ribas A. The evolution of checkpoint blockade as a cancer therapy: what's here, what's next? *Curr Opin Immunol.* 2015;33:23-35.
73. Emens LA, Kok M, Ojalvo LS. Targeting the programmed cell death-1 pathway in breast and ovarian cancer. *Curr Opin Obstet Gynecol.* 2016;28:142-147.
74. Sun WY, Lee YK, Koo JS. Expression of PD-L1 in triple-negative breast cancer based on different immunohistochemical antibodies. *J Transl Med.* 2016;14:173.

**How to cite this article:** Demeule M, Charfi C, Currie J-C, et al. TH1902, a new docetaxel-peptide conjugate for the treatment of sortilin-positive triple-negative breast cancer. *Cancer Sci.* 2021;112:4317-4334. <https://doi.org/10.1111/cas.15086>